Numerical studies of turbulent flames in wall-jet flows

by

Zeinab Pouransari

March 2015
Technical Reports from
Royal Institute of Technology
Department of Mechanics
SE-100 44 Stockholm, Sweden

Akademisk avhandling som med tillstånd av Kungliga Tekniska Högskolan i Stockholm framlägges till offentlig granskning för avläggande av teknologie doktorsexamen torsdagen den 12 mars 2015 kl 10.15 i F3, Kungliga Tekniska Högskolan, Lindstedsvägen 26, Stockholm.

Tryckt av Eprint-AB, Stockholm 2015

To Amin
and our children

Numerical studies of turbulent flames in wall-jet flows

Zeinab Pouransari
Linné FLOW Centre, KTH Mechanics, SE-100 44 Stockholm, Sweden

Abstract

The present thesis deals with the fundamental aspects of turbulent mixing and non-premixed combustion in the wall-jet flow, which has a close resemblance to many industrial applications. Direct numerical simulations (DNS) of turbulent wall-jets with isothermal and exothermic reactions are performed. In the computational domain, fuel and oxidizer enter separately in a non-premixed manner and the flow is compressible, fully turbulent and subsonic. The triple "turbulence-chemistry-wall" interactions in the wall-jet flow have been addressed first by focusing on turbulent flow effects on the isothermal reaction, and then, by concentrating on heat-release effects on both turbulence and flame characteristics in the exothermic reaction. In the former, the mixing characteristics of the flow, the key statistics for combustion and the near-wall effects in the absence of thermal effects are isolated and studied. In the latter, the main target was to identify the heat-release effects on the different mixing scales of turbulence. Key statistics such as the scalar dissipation rates, time scale ratios, two-point correlations, one and two-dimensional premultiplied spectra are used to illustrate the heat release induced modifications. Finer small mixing scales were observed in the isothermal simulations and larger vortical structures formed after adding significant amounts of heat-release. A deeper insight into the heat release effects on three-dimensional mixing and reaction characteristics of the turbulent wall-jet flow has been gained by digging in different scales of DNS datasets. In particular, attention has been paid to the anisotropy levels and intermittency of the flow by investigating the probability density functions, higher order moments of velocities and reacting scalars and anisotropy invariant maps for different reacting cases. To evaluate and isolate the Damköhler number effects on the reaction zone structure from those of the heat release a comparison between two DNS cases with different Damköhler numbers but a comparable temperature-rise is performed. Furthermore, the wall effects on the flame and flow characteristics, for instance, the wall heat transfer; the near-wall combustion effects on the skin-friction, the isothermal wall cooling effects on the average burning rates and the possibility of formation of the premixed mode within the non-premixed flame are addressed. The DNS datasets are also used for *a priori* analysis, focused on the heat release effects on the subgrid-scale (SGS) statistics. The findings regarding the turbulence small-scale characteristics, gained through the statistical analysis of the flow have many phenomenological parallels with those concerning the SGS statistics. Finally, a DNS of turbulent reacting wall-jet at a substantially higher Reynolds number is performed in order to extend the applicability range for the conclusions of the present study and figuring out the possible differences.

Descriptors: Turbulence, combustion, direct numerical simulation, wall-jet, heat release effects, mixing scales, non-premixed flame, wall heat transfer

Numeriska studier av turbulenta flammor i väggstråleströmning

Zeinab Pouransari
Linné FLOW Centre, KTH Mechanics, SE-100 44 Stockholm, Sweden

Sammanfattning

Denna avhandling behandlar fundamentala aspekter av turbulent blandning och sk "non-premixed" förbränning (dvs där syre och bränsle från början är separerade) i väggstråleströmning, vilket har starka likheter med många industriella tillämpningar. Direktsimulering (DNS) har genomförts av väggstråleströmning med isoterma såväl som exoterma reaktioner. I beräkningsdomänen kommer bränsle och syre in separat och strömningen r kompressibel, fullt turbulent och subsonisk. Den trefaldiga växelverkan mellan turbulens, kemiska reaktioner och vägg i väggstråleströmningen har behandlats, först med fokus på turbulenta strömningseffekter på en isoterm reaktion och sedan, genom att fokusera på reaktionens värmeavgivningseffekter både på turbulensen och flamegenskaperna i det exoterma reaktionsfallet. I det första fallet isoleras och studeras de viktigaste statistiska förbränningsrelaterade storheterna och väggnära effekter i frånvaro av termiska effekter. I det senare fallet var huvudsakliga målet att identifiera värmeutvecklingseffekter på de olika turbulenta blandningslängdskalorna. Viktiga storheter som skalärdissipationshastighet, tidsskalekvoter, tvåpunktskorrelationer, en- och tvådimensionella förmultiplicerade spektra används för att illustrera modifieringar inducerade av värmeavgivningseffekter. De små blandningslängdskalorna studerades i de isoterma simuleringarna och större virvelstrukturer kunde identifieras i de exoterma fallen. En djupare insikt i värmeavgivningseffekter på tredimensionella blandnings- och reaktionsegenskaper för den turbulenta väggstrålen har nåtts genom att använda DNS-data för att undersöka olika längd och tidsskalor. Speciellt har vi analyserat anisotropinivåer och intermittens genom att undersöka sannolikhetsfördelningar, högre ordningens moment av hastighets- och skalärfluktuationer samt anisotropiinvariantområden för olika fall med kemiska reaktioner. För att utvärdera och isolera effekten av Damköhlertal på reaktionszonstrukturen från de som orsakas av värmeavgivning så gjordes en jämförelse mellan två DNS-fall med olika Damköhlertal men med jämförbara nivåer av temperaturökning. Dessutom adresserades väggeffekter på flamman och på strömningskarakteristika, t.ex. värmeöverföring till väggen, effekter av väggnära förbränning på väggfriktion, de isoterma väggkylningseffekterna på genomsnittliga reaktionshastigheter och möjligheten till formering av s.k. förblandad förbränningsmod. DNS-databaserna användes också för a priori analys, fokuserad på värmeavgivningseffekter på "sub-grid-skale"-(SGS)-statistik. Resultaten angående statistik för små turbulensskalor, som fåtts genom statistisk analys av strömningen, har många fenomenologiska paralleller med de för SGS-statistik. Slutligen, en simulering av en väggstråle med kemiska reaktioner genomfördes med substantiellt högre Reynolds tal för att utöka det analyserade parameterområdet och för att studera möjliga Reynoldstalseffekter.

Preface

The present thesis deals with the fundamentals of turbulent mixing and non-premixed combustion in wall-jet configurations. An introduction to turbulent combustion simulations and the turbulent wall-jet set-up is provided in the first part. The second part contains the following six papers.

Paper 1. Z. Pouransari, G. Brethouwer and A. V. Johansson, 2011
Direct numerical simulation of an isothermal reacting turbulent wall-jet
Physics of Fluids, **23**, 085104.

Paper 2. Z. Pouransari, L. Vervisch and A. V. Johansson, 2013
Heat release effects on mixing scales of turbulent reacting wall-jets: a direct numerical simulation study
International Journal of Heat and Fluid Flow, **40**, pp. 65–80.

Paper 3. Z. Pouransari, L. Bifelare and A. V. Johansson, 2015
Statistical analysis of the velocity and scalar fields in reacting turbulent wall-jets
Physics of Fluids, **27**, 025102.

Paper 4. Z. Pouransari, L. Vervisch, L. Fuchs and A. V. Johansson, 2015
DNS analysis of wall heat transfer and combustion regimes in a turbulent non-premixed wall-jet flame
To be submitted.

Paper 5. Z. Pouransari, A. Rasam, L. Vervisch and A. V. Johansson, 2015
Assessment of subgrid-scale stress statistics in non-premixed turbulent wall-jet flames
To be submitted.

Paper 6. Z. Pouransari, L. Vervisch and A. V. Johansson, 2014
Reynolds number effects on statistics and structure of an isothermal reacting turbulent wall-jet
Flow, Turbulence & Combustion, **92**, pp. 931–945.

Division of work between authors
The advisor of the project has been Prof. Arne V. Johansson (AJ) and Prof. Luc Vervisch (LV) has acted as the external honorary advisor. Prof. Luca Biferale (LB), Dr. Amin Rasam (AR), Prof. Laszlo Fuchs (LF) and Dr. Geert Brethouwer (GB) are the coauthors in different papers.

Paper 1.
Numerical simulations were performed by Zeinab Pouransari (ZP). Discussion was being held between ZP, GB and AJ for interpretation of the results. The paper was written by ZP with feedback from AJ and GB.

Paper 2.
Development of the relevant subroutines was done by ZP. Numerical simulations and interpretation of results were carried out by ZP in collaboration with AJ. Paper was written by ZP with input from LV and AJ.

Paper 3.
The idea of the paper was initiated by ZP with input from LB. Paper was written by ZP and feedback and comments were provided by LB and AJ.

Paper 4.
The idea was born while ZP was visiting LV in France. Numerical simulations were performed by ZP. Paper was written by ZP and feedback and comments were provided by LV, LF and AJ.

Paper 5.
The idea of the paper was developed by ZP in discussion with LV, AR and AJ. Development of the relevant subroutines was done by ZP. Paper was written by ZP and AR and feedback and comments were provided by LV and AJ.

Paper 6.
Numerical simulations were performed by ZP with input from AJ. Paper was written by ZP and feedback and comments were provided by LV and AJ.

Contents

Part I

Introduction

CHAPTER 1

Overview

The industrial power available to mankind is still mainly provided by the chemical energy stored in hydrocarbon fossil fuels. The combustion process, through which the fuel is burned and the chemical energy is released, is of crucial importance to almost every engineering process. A truly remarkable progress has been made in the field of combustion and there have been excellent recent improvements both in measurements and numerical simulations of reacting flows with detailed chemistry. However, many new combustion devices are expected to work in previously unexplored ranges. Thus, there is a continuous need to advance our understanding of the full burning process.

To shed light into the fine grained interactions tangled in the turbulent reacting flows especially, in the near-wall region, perhaps only direct numerical simulation (DNS) can be an appropriate candidate for high fidelity computations. In DNS, all the flow scales as well as the flame structure are meant to be resolved. The exact definition of DNS in reacting flows is a subject of further discussion, which will briefly be addressed in chapter 3.

Many combustion applications in confined domains contain regions where mixing and reaction take place close to a wall. Thus, a better understanding of the wall effects plays an essential role in gaining insight into the full problem. The turbulent plane wall-jet flow has a close resemblance to a wide range of mixing and combustion applications. In particular, the interactions of reaction and mixing with walls are of great interest in the wall-jet configuration. A schematic of a turbulent plane wall-jet flow is given in figure 1.1, which shows instantaneous snapshots of temperature and streamwise velocity fields. The structure of a developed turbulent wall-jet can formally be described as two adjacent shear layers of different character. The small scales of turbulence are present close to the wall, whereas larger scales exist in the outer shear region, and this makes the turbulent wall-jet a valuable test case for reaction and mixing applications.

In the present study, the main objective is to examine the triple interactions between turbulent mixing, chemical reaction and wall effects. The primary target is to investigate the mixing characteristics together with the near-wall behavior of the reacting species as well as the reaction rate in the turbulent reacting wall-jet configuration. The present study is not intended to present a realistic chemical reaction, but is rather an exploratory study to demonstrate the fundamental mixing and reaction characteristics by analyzing

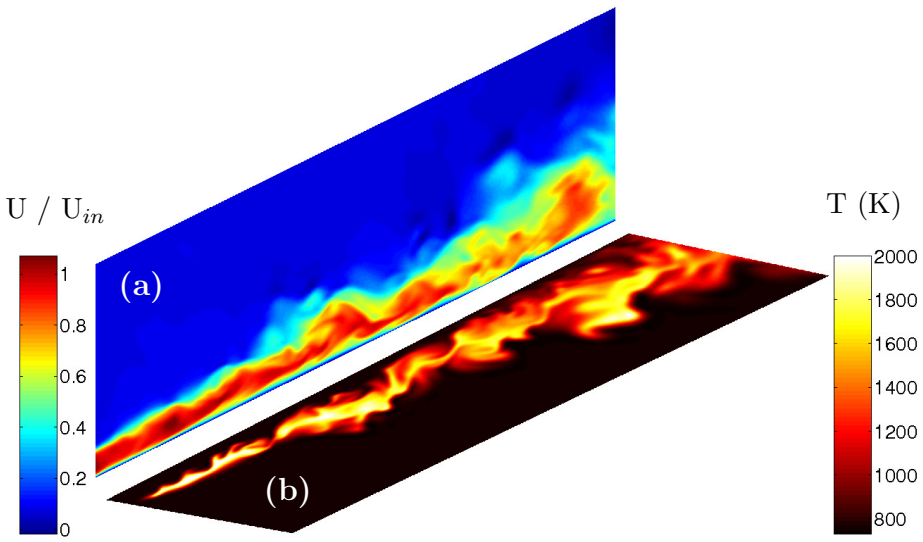

FIGURE 1.1. Snapshots of the instantaneous streamwise velocity (upper) and temperature (lower) fields for a reacting turbulent plane wall-jet flow, taken from Pouransari *et al.* (2013). The flow is from left to right, U_{in} is the jet inlet velocity and temperatures are in Kelvin.

the key statistics for combustion, such as the probability density functions, higher order moments of the scalar concentrations, turbulent kinetic energy and scalar dissipation rates.

In order to do so, the investigation is started by performing DNSs of an isothermal reacting turbulent wall-jet flow. In the first part of this study, the flow is uncoupled from the reaction and the influence of turbulent mixing on the reaction is studied in the absence of temperature effects. This part of our study intentionally disregards the effects of chemical reactions on the turbulent flow field and concentrates on the turbulent flow effects on the isothermal reaction. The focus is on mixing properties, which gives a valuable material for comparison to the following study, where heat-release is added.

In the second phase of this study, exothermic reactions are considered and DNSs of turbulent reacting wall-jets including significant amounts of heat-release are performed. The heat-release effects are indeed very important in reacting flows in general and also in the present turbulent wall-jet set-up. Moreover, the flame-wall interactions are of crucial importance, both in the isothermal reaction framework and even more, in the presence of the heat-release effects, as was mentioned earlier. Thus, in this part, we have concentrated more on the heat-release effects on the turbulent flow field and turbulence-chemistry

interactions present in the turbulent wall-jet configuration, including the near-wall behavior.

In the next step of this investigation, the DNS databases obtained from various reacting wall-jet simulations are used for further investigations on different aspects of the triple interactions. For instance, though the general heat release effects on the dynamics of the turbulent wall-jet flow were addressed, we attempted to get a deeper insight into the heat release effects on the turbulence structures and anisotropy levels. Similar to many other fundamental researches, this part of the investigation may not directly have implications for mixing and combustion applications and is of more interest in a theoretical perspective. However, we argue that the combined effects of strong intermittency and strong persistency of anisotropy at the small scales in the entire computational domain of the turbulent wall-jet flow can affect mixing and ultimately the combustion characteristics of the reacting flow.

For the next stage of the project development, the important objective was the detailed study of the wall effects. Even though different turbulence and combustion characteristics were addressed close to the wall, throughout the entire project, but still paying a special attention to the wall effects seems to be of a great value in improving our understating of the near-wall flame characteristics in the turbulent wall-jet flow. With experiences gained from the earlier stages of this research, new sets of DNSs are performed in a larger computational domain than the preceding studies and hence, there is more room to study the turbulence-wall and flame-wall interactions. In particular, this part of the study focuses on the wall heat transfer, the skin friction development and wall cooling effects on the near-wall flame characteristics.

In a further step of the project, the DNS databases are used to investigate the heat release effects on the geometry of the subgrid-scale (SGS) quantities, such as the stress tensor and its relative alignment with the resolved strain-rate tensor as well as its anisotropy are investigated. Furthermore, the behavior of the SGS dissipation of turbulent kinetic energy and enstrophy in the presence of heat release effects is addressed. The purpose of this study is to provide valuable information about the heat release effects on the SGS stress tensor statistics, which is indeed important for the design of SGS models.

Finally, in order to examine whether or not the outcomes of the present study are limited to the particular Reynolds numbers of the investigation, DNS at a substantially higher Reynolds number is performed and the results are compared to the previous ones and generalized to a wider range of Reynolds numbers.

The remainder of this exposition is organized as follows. Chapter 2 provides an introduction to turbulent combustion, which includes a brief review of turbulence, combustion and their interactions. Chapter 3 is devoted to the simulation and modeling issues that need to be addressed for the purpose of the present numerical investigation. The governing equations for the flow field as well as the basic equations for the chemical reaction are exhibited. The

fundamentals of the turbulent reacting flow simulations and different numerical approaches are introduced here. In this chapter, the turbulent combustion simulation is addressed in a general sense with the emphasis on DNS of non-premixed turbulent reacting flows and in particular those studies that involve flame-wall interactions. Moreover, some basics of combustion modeling tools are included. This part is intentionally kept brief and only those issues which are of relevant importance for the DNS data analysis are accentuated. The turbulent wall-jet flow is introduced in chapter 4, where different types of wall-jet configurations are described. Besides, different scalings, which are used for presenting the results are introduced and discussed. Some parts of the results, both from the isothermal and exothermic reacting cases are included in this chapter. Chapter 5 is devoted to the heat release effects on the flow and flame structure of the reacting turbulent wall-jet flow. A summary of the papers, presented in part II of this thesis, can be found in chapter 6 and is followed by the concluding remarks and outlook for the future research in chapter 7.

CHAPTER 2

Introduction to turbulent combustion

2.1. Turbulence

2.1.1. *Introduction to turbulent flows*

Flows in nature and in engineering applications are mostly turbulent. Turbulence is characterized by the presence of random and chaotic three-dimensional vorticity fluctuations in space and time. Turbulence occurs at high Reynolds numbers and is dissipative, meaning that if no energy is supplied, it decays rapidly. Turbulence is one of the most complex problems in fluid mechanics, however, this does not stop us from challenging ourselves for gaining authority over the world around us and finding the solution to some set of equations that govern the problem (Tennekes & Lumley 1972).

To understand the problem easier, flow visualizations are often used to illustrate turbulent flows. Figure 2.1 shows a snapshot of the instantaneous passive scalar field in a turbulent wall-jet flow. It exhibits the existence of a wide range of length scales, an important characteristic of turbulent flows. To describe these scales a mathematical theory is needed. Moreover, understanding the manner in which these scales are related to each other and exchange energy has a great significance in our perspective of turbulent flows (Davidson 2004).

From the early flow visualizations, a cascade process was proposed in which the large eddies break down into ever smaller eddies (Richardson 1922). This picture is indeed very close to what happens in the real world; even though it is not yet completely clear how the energy is transferred between different scales. There exist some reverse energy transfer from small to large scales, but the net energy transfer is from large to small scales and the energy definitely ends up at the dissipative scales where the viscosity dominates.

There are strong interactions between scales with an interesting energy transfer mechanism. The size of the largest vortical structures, containing most of the turbulence energy, is essentially limited by geometrical restrictions, for instance, the boundary layer thickness in turbulent boundary layers. The dissipation of turbulence energy mostly takes place at the smallest scales, which are assumed to be independent of the flow geometry and depend only on the viscosity and viscous dissipation. These scales are referred to as the Kolmogorov

FIGURE 2.1. A snapshot of the instantaneous passive scalar field in turbulent reacting wall-jet flow, from the DNS database of Pouransari *et al.* (2014).

scales, see Kolmogorov (1941). The Kolmogorov length scale is defined as

$$\eta = \left(\frac{\nu^3}{\epsilon}\right)^{1/4}. \tag{2.1}$$

Another practical length scale in the study of turbulence is the Taylor micro scale (Pope 2000), that can be defined as

$$\lambda = \sqrt{\frac{15\nu}{\epsilon}u_{rms}^2}, \tag{2.2}$$

where ϵ is the viscous dissipation rate. The Taylor micro scale λ is larger than the Kolmogorov micro scale η that was introduced and is not a dissipation length scale, as it is defined with the aid of the turbulence velocity.

2.1.2. *Scalar turbulence*

In addition to turbulent flows, the advection of a scalar, e.g. a passive substance or temperature fluctuations, by the turbulent flow is important in many natural and engineering flows, especially in combustion systems. The scalar concentration exhibits a complicated dynamical behavior that has many similarities with that of the turbulent velocity field. The complex aspects of the scalar characteristics apparently arise from the mixing process rather than the turbulent velocity field (Shraiman & Siggia 2000), and the scalar field is mainly decoupled from the velocity field, see figure 2.2.

Passive scalar turbulence has recently yielded to mathematical analysis, and such progress may ultimately lead to a better understanding of the still intractable problem of fluid turbulence itself. Concerning scalar and temperature gradient fluctuations, the available data and discussions are even more diverse and complicated than for the turbulent velocity field. Already, the behavior of the passive scalar statistics is non-trivial and still a major field of research (Falkovich *et al.* 2001).

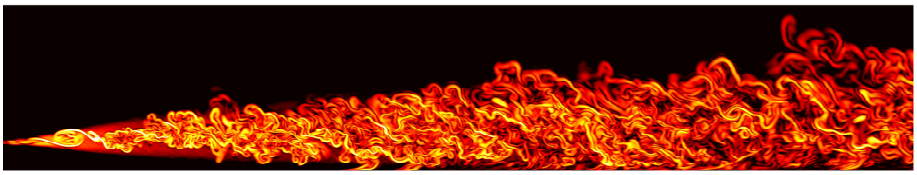

FIGURE 2.2. A snapshot of the scalar dissipation rate field in turbulent reacting wall-jet flow, from the DNS database of Pouransari *et al.* (2014).

2.1.3. *Statistical tools for analysis of turbulence*

Stochastical techniques and statistical analysis, which are mostly based on the idea of averaging, are often used to study turbulent flows (Monin & Yaglom 1975; Lumley 2007).

Consider a dynamic quantity $\varphi(x,t)$, representing e.g. a velocity component, temperature or the chemical species concentration. Here x is the vector denoting the spatial coordinates and t is time. The Reynolds average of φ, denoted by $\overline{\varphi}$, can be defined as an ensemble, spatial, and/or temporal average, depending on the problem. In turbulent flow studies, it is often convenient to use the Reynolds decomposition as

$$\varphi = \overline{\varphi} + \varphi', \tag{2.3}$$

where φ' is the fluctuation about the mean value. In the case of variable density flows, alternatively density-weighted or Favre-averaged values can be used, denoted by $\widetilde{\varphi} = \overline{\rho\varphi}/\overline{\rho}$, where $\rho(x,t)$ is the fluid density. If Favre averaging is used, φ is decomposed as

$$\varphi = \widetilde{\varphi} + \varphi'', \tag{2.4}$$

where φ'' is the fluctuation about the density-weighted average and $\widetilde{\varphi}$ denotes the density-weighted mean.

The frequency of occurrence of a given value from a number of realizations of a random variable can be displayed by dividing the range of possible values into a number of bins. A histogram is illustrated and its shape depends on the statistical distribution of the random variable, the total number of realizations and also the size of the bins. If the number of realizations increases while the bin size goes to zero, the histogram goes to a limiting curve called the probability density function (PDF) of the random variable. A complete statistical description of a stochastic function would be provided by a PDF, which provides a one-point statistical information about the random variable. This random field may, for instance, be the concentration level of a chemical species. To describe the turbulent combustion processes it is necessary to collect information about the behavior of the chemical species throughout the entire simulation domain. From this point of view, the statistical description

provided by the PDF is a method to zoom in on any particular interesting zone and collect selective data, also on the subgrid-scale level that can be input to combustion models for large eddy simulation.

The variance is defined as the second central moment of the random variable,

$$\varphi_{rms}^2 = \widetilde{(\varphi - \widetilde{\varphi})^2}. \tag{2.5}$$

Clearly, the first and second moments are the most important quantities for the interpretation of the turbulent flow state. However, the changing shape of the PDFs of a variable strongly influences the corresponding higher order moments. The normalized generalized skewness of order n is defined as

$$S_\varphi^{(n)} = \frac{\overline{(\varphi'')^{(2n+1)}}}{\overline{(\varphi'')^2}^{(2n+1)/2}}, \tag{2.6}$$

where with $\varphi'' = \varphi - \widetilde{\varphi}$ the fluctuation of any scalar field around its Favre-averaged mean value is denoted.

The first non-trivial case, $n = 1$ is typically called the skewness of a field and the dependency on the index (n) is dropped. Concerning a vector field, the skewness defined in terms of any of its components would be zero in an isotropic field. To characterize the intense non-Gaussian properties of the field, independent of its isotropic or anisotropic content, it is useful to introduce the generalized flatness factor of order n:

$$F_\varphi^{(n)} = \frac{\overline{(\varphi'')^{(2n+2)}}}{\overline{(\varphi'')^2}^{(2n+2)/2}}, \tag{2.7}$$

which is a proxy of the degree of departure from a purely Gaussian shape (Frisch 1995). For instance for the simplest case $n = 1$, in a Gaussian distribution $F^{(1)} = 3$.

2.2. Combustion

2.2.1. *The oldest technology of mankind*

Combustion is the oldest technology of mankind and has been the major source of energy for more than one million years and seemingly is going to remain an important subject as long as the human civilization exists. Combustion is an applied science that is important in transportation, power generation, industrial processes, chemical engineering and aeronautical applications. Today, the number of combustion systems used in transportation and transformation industries is rapidly growing. People want to travel faster and at the same time pollution and environmental problems are becoming critical issues in our societies. The negative environmental impacts of excessive fossil fuel combustion are becoming evident. Emissions of CO_2 contribute to global warming. Other pollutants such as unburnt hydrocarbons, soot and nitrogen oxides also have a negative impact on the environment. More rigorous regulations concerning emissions are presently enforced in the automotive industry and on power

plants to reduce emissions and their environmental impact. Thus, we need to improve our combustion technology accordingly. To reach these goals, an improved understanding of combustion and mixing processes, as well as improved models to be used in the development of cleaner combustion applications are needed (Williams 1985; Turns 1993; Glassman & Yetter 2008).

2.2.2. *Chemical reaction*

Our knowledge about the gas reactions in general and the combustion of fuels in particular has substantially improved. There is a large body of publications about elementary reaction mechanisms and their rate data. From a "chemist" point of view, a simplified reaction model can consist of a hundred reactions and more than twenty species. For instance, a mechanism for methane oxidation comprises 77 reactions and 49 species. However, there are a lot of different methods to reduce the number of independent variables in a mechanism, and a lot of efforts have been undertaken to develop reduced mechanisms for fuel combustion. The reduced mechanisms are very useful for numerical simulation purposes, as they decrease the data storage and computational resource requirements. Nonetheless, in the numerical simulations with fluid dynamical aspects a single step global reaction is often used. A single-step global reaction is only a coarse approximation of the chemistry occurring in the real life, even for simple chemical reactions, but it allows us to study the interactions between the heat-release and turbulence in a real three-dimensional flow. It is a very useful methodology to gain insight into the generic characteristics and effects of a chemical mechanism in different flow fields. Using DNS together with the simple chemistry has been a customary approach to address combustion problems and it has been frequently used to study different flow fields.

2.2.3. *Experimental or numerical approach*

Turbulent reacting flows in general and combustion systems in particular have been tackled both numerically and experimentally. The experimental works have advanced our understanding of the turbulent combustion systems enormously in the past decades. Modern investigations of turbulent flames were probably initiated by the theoretical and experimental study by Damköhler (1947). Although, the recent simultaneous measurements of turbulent velocity fields and the reacting scalar concentrations together with local temperature, has helped us to gain a more realistic picture of the burning process. However, obtaining detailed information from high quality computations seems to be necessary for gaining insight into the fundamentals of the physics of the turbulence-chemistry interaction. A considerable amount of time and expensive experimentation can be saved with the help of the computational analysis. Moreover, numerical simulations statistics can be treated as an equivalent of controlled accurate experimental datasets. An important practice is to implement the state-of-the-art knowledge, gained from well designed numerical

simulations, into the combustion models. Performing a similar task with an experimental dataset would be much more difficult and expensive.

2.2.4. *Chemical engineering or fluid mechanics viewpoint*

To study turbulent reacting flows, a good knowledge of both turbulence and combustion is necessary. In order to understand how the fluid flow affects the chemistry one must have an excellent understanding of turbulent flows and turbulent mixing. In addition, an equally good understanding of chemistry is required. A brief review of the literature in these areas will quickly reveal the complexity of the task (Fox 2003). Different approaches have been developed for dealing with turbulent reacting flows. These differences mainly arise from the relevant importance of different aspects. The main approaches that can be considered are the reaction engineering approach and the fluid mechanic approach. In the former, the focus is mainly on the chemistry and the fluid flow effects are of much less significance (Warnatz *et al.* 2006). While in the latter, the emphasis is on how the fluid flow affects the flame (Fox 2003; Cant & Mastorakos 2007). One of the primary factors in determining the most appropriate approach in various problems is the relative characteristic time scale of the chemical reaction to the turbulence time scale. When the chemical time scales are larger than the turbulence time scale, the details of the flow can safely be ignored. Likewise, when chemical time scales are much smaller than the turbulence time scale, the details of the chemical kinetics are assumed to be of less importance. However, an accurate description of both the turbulent flow and chemistry is required for obtaining a full insight of the problem. In the present study, the second approach is used and we concentrate on how the heat released by the reaction interacts with the turbulent flow.

2.2.5. *Premixed and non-premixed regime*

Studying the mechanisms involved in turbulent combustion flows has been the objective of numerous theoretical, experimental and numerical works in the last century. Combustion can be classified according to several criteria and one of the most common classifications is made depending on the way the reactant species are mixed prior to entering the combustion chamber. Consequently, the academic universe of combustion science is divided into non-premixed and premixed combustion regimes, where in the former, fuel and oxidizer are separated prior to burning and in the latter, they are mixed before ignition. Turbulent premixed flames are present in spark-ignited engines and in combustion chambers of power plant turbines while examples of non-premixed flames are the diesel engines, boiler furnaces and rocket engines. In turbulent non-premixed jet flames, when a jet fuel is injected into the air, the turbulent flow causes the entrainment of the air into the fuel jet and subsequently the turbulent flame length becomes independent of the jet velocity. However, one needs to be aware of the fact that this division is more of an academic importance and a definite border does not exist in practical situations and many fuels burn in partially

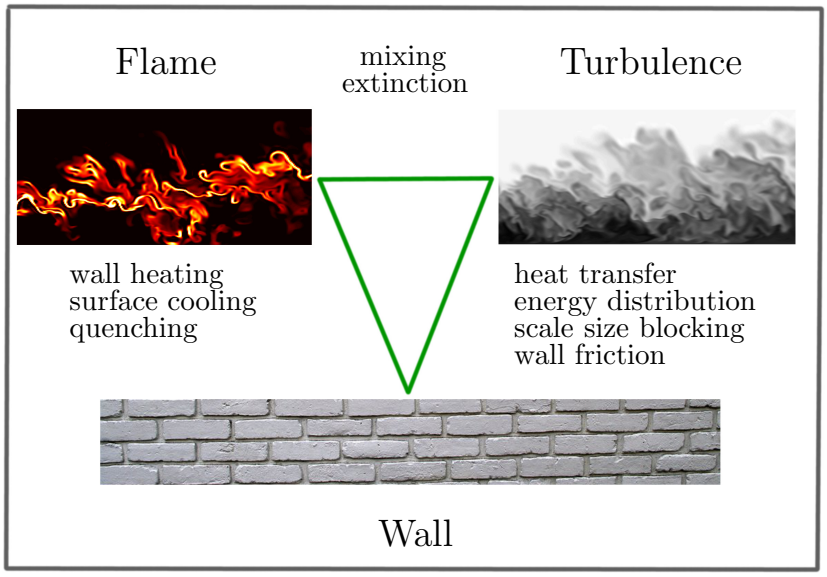

FIGURE 2.3. The triple interaction between the wall, turbulence and combustion.

premixed conditions. The present work deals with a non-premixed case, which is also more widely used in industrial applications, due to safety reasons.

2.3. Turbulence-flame-wall interactions

2.3.1. *The triple interactions*

The combustion mechanism needs to be understood together with turbulence for two reasons. Turbulence increases the mixing process and enhances combustion, on the other hand, combustion releases heat which generates gas expansion and buoyancy variation that influences the turbulent flow. While the mixing process in turbulent flows is known to be associated with the local strain rate, the details of the mixing process in turbulent flows remain to be explained more quantitatively. Besides, the structure of the turbulent flow is not yet fully understood and the mixing prediction remains to be a challenge. The unresolved problems in turbulence seem to become even more complicated in turbulent combustion systems. The interaction of turbulent mixing with chemical reaction is even less explored. Moreover, this interaction can get substantially affected by the presence of the walls, which is the case in most combustion systems. Walls affect turbulence through a number of different mechanisms and at the same time, the flame structure is affected by walls, see Perot & Moin (1995) and the references therein for a review on the near-wall turbulence. Some of these interactions are outlined in figure 2.3.

In practice, combustion must simultaneously be safe, efficient and clean. Thus, different interactions involved in the turbulent reacting flows need to be understood, in order to enhance different aspects of the performance of the combustion systems. To burn as efficient as possible, we need to mix better and at the same time take care of the flame stability, all these are not possible without obtaining accurate information about the turbulent flow field.

2.3.2. *Wall heat transfer*

The wall heat transfer and shear stress are two major important quantities of interest in industrial flows, including combustion problems. Understanding the heat-release effects on the wall heat transfer and skin friction coefficients in turbulent reacting flows is essential for a wide variety of industrial flows, especially combustion problems. In many combustion applications, regions exist where mixing and reaction take place close to a wall and affect the wall quantities leading to the unsteady wall heat transfer caused by the near-wall turbulence. The study of wall heat transfer and possible different Reynolds analogy formulations in compressible wall-bounded turbulent flows has been of interest for decades and is still an ongoing field of research (Huang *et al.* 1995; Peters 2000; Pitsch 2010; Zhang *et al.* 2014). To achieve the optimum design of the heat transfer equipments in general, it is important to consider that the heat transfer mechanisms can be affected by the flow configuration parameters and temperature ratio distribution over the target surface. In particular, to achieve a high wall heat transfer rate in turbulent wall-jet flows, a detailed knowledge is required not only of the wall-heat flux rates, but also of the isothermal surface conditions. Thus, significant improvements can be achieved by modification of the wall conditions. Moreover, understanding the dynamics of the turbulence structures and the physical dynamics of the problem, in the near-wall region, is crucial for analyzing mixing, heat transfer, drag reduction and other phenomena, and has an impact on the overall Nusselt number.

Both turbulent and laminar wall-jet flows are widely used for various cooling and heating purposes in engineering applications and several studies have been performed to understand the underlying heat transfer mechanisms (Seidel & Fasel 2001). According to the industrial needs, curved or plane wall-jets may be used for various cooling applications. In particular, the turbulent wall-jet flows have been acknowledged for their capability in achieving significant wall heat and mass transfer rates. In the turbulent wall-jet flow, the wall heat transfer is influenced by the unsteady dynamics of the velocity field and, generally, the complex dynamics of the flow has a promotive effect on the total wall heat transfer, compared to that of the boundary layer.

CHAPTER 3

Simulation and modeling of turbulent reacting flows

3.1. An overview of turbulent combustion simulation

Performing any kind of turbulent combustion simulation is a challenging task for various reasons. Combustion has a strong multi-scale and non-linear nature and a wide range of length and time scales are involved, which add to the broad spectrum of turbulence scales. In addition, large numbers of species are involved in any reacting flow, even in the simplest combustion processes, bringing further complexity to the problem. Besides, combustion processes in the real world situations usually occur in multiphase environments, with presence of thermal radiation and acoustic effects. Moreover, all these different phenomena are interacting with each other and tight couplings exist between them, see e.g. Hawkes *et al.* (2007). Therefore, in simulations of reacting flows, some types of simplifications need to be done. Depending on the priorities and important issues, these simplifications may be assumed for the flow aspects or for the chemistry involved. The description of the reactions, however, almost always has to be simplified. For instance, a complete mechanism for the simple reaction of hydrogen and oxygen gases typically involves 19 reactions and 9 species (Conaire *et al.* 2004). Many different numerical efforts have been undertaken to simulate turbulent combustion and numerous combustion models have been developed and used for various applications. However, industrial combustion systems are constantly changing and the next generation of combustion systems are likely to operate in previously unexplored regimes. Internal combustion engines and gas turbines may burn fuel at lower temperatures, higher levels of dilution and much less pollutant emissions. The reaction process in these new environments brings up complicated challenges. Therefore, better understanding of the fundamentals of combustion systems, in particular "turbulence-chemistry" interaction, seems to be necessary for achieving efficient burnings. An important practice is to implement our state-of-the-art knowledge, gained from DNS studies, into the models. We can of course get a lot of important and useful information from the direct simulations, however, learning the physics behind them in order to improve the models is not a trivial task, see Pitsch & Trisjono (2014). An overview of rather recent research interests, in the turbulent combustion computational and modeling community, is given by Bilger (2000). The application of detailed chemistry and transport models was reviewed and discussed by Hilbert *et al.* (2004).

3.2. Governing equations

In direct numerical simulation of turbulent reacting flows, the governing equations of compressible flow and transport equations for the participating species must be solved. In the following, the governing equations of a compressible reacting multicomponent fluid, containing n species, are presented. The notation follows Poinsot & Veynante (2005) and the derivations of the equations, based on the conservation of mass, momentum and energy, can be found in the reference works of Williams (1985) and Turns (1993).

3.2.1. *Conservation of mass and momentum*

The global mass conservation equation for compressible flows is expressed as

$$\frac{\partial \rho}{\partial t} + \frac{\partial \rho u_i}{\partial x_i} = 0, \tag{3.1}$$

where ρ is the mass density and u_i is the velocity vector.

The momentum conservation equation, valid for both reacting and non-reacting flows reads

$$\frac{\partial \rho u_i}{\partial t} + \frac{\partial \rho u_i u_j}{\partial x_j} = -\frac{\partial p}{\partial x_i} + \frac{\partial \tau_{ij}}{\partial x_j} + F_i. \tag{3.2}$$

Here, τ_{ij} represents the viscous stress tensor and F_i represents a body force. For a Newtonian fluid, τ_{ij} is defined as

$$\tau_{ij} = \mu \left(\frac{\partial u_i}{\partial x_j} + \frac{\partial u_j}{\partial x_i} \right) - \mu \frac{2}{3} \frac{\partial u_k}{\partial x_k} \delta_{ij}, \tag{3.3}$$

where μ is the dynamic viscosity. Assuming no body forces, the momentum equation becomes

$$\frac{\partial \rho u_i}{\partial t} + \frac{\partial \rho u_i u_j}{\partial x_j} = -\frac{\partial p}{\partial x_i} + \frac{\partial}{\partial x_j} \left[-\frac{2}{3} \mu \frac{\partial u_k}{\partial x_k} \delta_{ij} + \mu \left(\frac{\partial u_i}{\partial x_j} + \frac{\partial u_j}{\partial x_i} \right) \right]. \tag{3.4}$$

The viscosity is determined through the Sutherland's law

$$\frac{\mu(T)}{\mu_j} = \left(\frac{T}{T_j} \right)^{3/2} \frac{T_j + S_0}{T + S_0}, \tag{3.5}$$

where T is the local absolute temperature and the j-indices denote the jet reference condition[1]. For the wall-jets, a reference temperature of $S_0 = 110.4K$, valid for air at moderate temperatures and pressures, is used.

3.2.2. *Conservation of energy*

The energy conservation equation needs the most attention since many different forms exist. Here the governing equation for the total non-chemical energy the

[1]Not to be confused with the dummy index j in other equations.

sum of the internal and kinetic energy per unit mass $E = e + \frac{1}{2}u_i u_i$ is used, which reads

$$\frac{\partial \rho E}{\partial t} + \frac{\partial \rho E u_j}{\partial x_j} = \dot{\omega}_T - \frac{\partial q_i}{\partial x_i} + \frac{\partial (u_i(\tau_{ij} - p\delta_{ij}))}{\partial x_j} + \dot{\mathcal{Q}} + \rho \sum_{k=1}^{n} \theta_k f_{k,i}(u_i + V_{k,i}). \quad (3.6)$$

Here, $\dot{\omega}_T$ is the heat release term due to combustion, $\dot{\mathcal{Q}}$ is the heat added by external sources (e.g. an electric spark) and $V_{k,i}$ is the x_i-component of the diffusion velocity of the k^{th} species θ_k. The last term on the right hand side describes the power produced by a volume force $f_{k,i}$. The summation convention over repeated indices is used. The heat fluxes q_i are approximated by Fourier's law $q_i = -\lambda \frac{\partial T}{\partial x_i}$, where λ is the coefficient of thermal conductivity[2].

Assuming no external forces and heat sources in the flow and using Fourier's law the governing equation for the total energy is simplified to

$$\frac{\partial \rho E}{\partial t} + \frac{\partial \rho E u_j}{\partial x_j} = \dot{\omega}_T + \frac{\partial}{\partial x_j}\left(\lambda \frac{\partial T}{\partial x_j}\right) + \frac{\partial (u_i(\tau_{ij} - p\delta_{ij}))}{\partial x_j}. \quad (3.7)$$

A thermally perfect gas is assumed, and therefore the internal energy and enthalpy are only functions of the temperature,

$$\begin{aligned} e = e(T) \quad &\Longrightarrow \quad de = c_v dT, \\ h = h(T) \quad &\Longrightarrow \quad dh = c_p dT. \end{aligned} \quad (3.8)$$

Here, c_v and c_p are the specific heats at constant volume and pressure, respectively, which in general are functions of the temperature. If the specific heats are also assumed constant, the system is calorically perfect and

$$\begin{aligned} e &= c_v T, \\ h &= c_p T. \end{aligned} \quad (3.9)$$

The gas is assumed to be ideal and obey the perfect gas law

$$p = \rho R T, \quad (3.10)$$

where R is the specific gas constant. Using the definition of enthalpy and the perfect gas law, the specific heats can be expressed as

$$\begin{aligned} c_p &= \frac{\gamma R}{\gamma - 1} \\ c_v &= \frac{R}{\gamma - 1}, \end{aligned} \quad (3.11)$$

where $\gamma = c_p/c_v$. Using these relations, the pressure and temperature can be written as functions of the internal energy e

$$\begin{aligned} p = \rho R T = \rho R \frac{e}{c_v} &= (\gamma - 1)\rho e \\ T = \frac{p}{\rho R} &= \frac{(\gamma - 1)}{R}\, e. \end{aligned} \quad (3.12)$$

[2]Not to be confused with the Taylor micro scale.

The heat diffusion can be expressed as a function of the internal energy and the specific heat c_p using (3.12) and (3.11) as

$$q_j = -\lambda \frac{\partial}{\partial x_j}\left(\frac{(\gamma-1)e}{R}\right) = -\lambda \frac{\partial}{\partial x_j}\left(\frac{\gamma e}{c_p}\right). \tag{3.13}$$

Here, constant values of c_p, c_v and γ are considered. The heat diffusion is often defined in terms of the Prandtl number Pr, relating the momentum and heat transport

$$Pr = \frac{\nu}{\lambda/(\rho c_p)} = \frac{\mu c_p}{\lambda}. \tag{3.14}$$

Using this definition, the energy flux can be expressed as

$$q_j = -\frac{\gamma\mu}{Pr}\frac{\partial e}{\partial x_j} \tag{3.15}$$

and the energy equation, in terms of $E_t = \rho E$, for an ideal gas becomes

$$\frac{\partial E_t}{\partial t} + \frac{\partial E_t u_j}{\partial x_j} = \dot{\omega}_T + \frac{\partial}{\partial x_j}\left[\frac{\gamma\mu}{Pr}\frac{\partial}{\partial x_j}\left(\frac{E_t}{\rho} - \frac{1}{2}u_i u_i\right)\right] + \frac{\partial(u_i(\tau_{ij} - p\delta_{ij}))}{\partial x_j}. \tag{3.16}$$

3.2.3. *Conservation of species mass*

A convenient approach for the species conservation is to utilize the species mass fractions of the mixture defined by

$$\theta_k = \frac{m_k}{m} = \frac{\rho_k}{\rho}, \tag{3.17}$$

where m_k is the mass of the k^{th} species in a given volume V and m is the total mass in this volume. Each of the species obeys a mass transport equation of the form

$$\frac{\partial \rho\theta_k}{\partial t} + \frac{\partial}{\partial x_i}\left[\rho\theta_k(u_i + V_{k,i})\right] + \dot{\omega}_k = 0, \tag{3.18}$$

where $V_{k,i}\,\theta_k$ is the diffusive flux in the i^{th}-direction, and $\dot{\omega}_k$ is the mass reaction rate describing the rate of creation or destruction of the species. Diffusive fluxes are caused by a number of transport processes on the molecular level. Accounting for all these is often computationally too expensive. The most common approximation is to assume that the fluxes follow the Fick's law

$$V_{k,i}\theta_k = -\mathcal{D}_k \frac{\partial \theta_k}{\partial x_i}, \tag{3.19}$$

where $\mathcal{D}_k$ is the diffusion coefficient of species k. Using this approximation, the species conservation equation takes the form

$$\frac{\partial \rho\theta_k}{\partial t} + \frac{\partial}{\partial x_j}\left(\rho\theta_k u_j\right) = \frac{\partial}{\partial x_j}\left(\rho\mathcal{D}\frac{\partial \theta_k}{\partial x_j}\right) + \dot{\omega}_k, \tag{3.20}$$

where θ_k and $\dot{\omega}_k$ are the mass fractions and reaction rates of the oxidizer, fuel and passive scalar species. An equal diffusion coefficient, $\mathcal{D}_k = \mathcal{D}$, for all scalars is used to approximate the diffusive fluxes. The $\mathcal{D}_k$ coefficients are often characterized in terms of the Lewis number, $Le_k = \frac{\lambda}{\rho C_p \mathcal{D}_k}$.

3.2.4. *Single-step irreversible chemical reaction*

A single-step reaction involving N species can be described by

$$\sum_{k=1}^{N} \nu_k^r \mathcal{M}_k \rightarrow \sum_{k=1}^{N} \nu_k^p \mathcal{M}_k, \tag{3.21}$$

where $\mathcal{M}_k$ denotes the concentration of the k^{th} species in moles per unit volume, ν_k^r are the stoichiometric coefficients of the reactants and ν_k^p are the stoichiometric coefficients of the products. Consider a simple case where reaction involves only the oxidizer species O and fuel species F that react to form a product P which is described as

$$F + r\,O \longrightarrow (1+r)\,P. \tag{3.22}$$

The mass fraction θ_k of each species (O, F and P) follows the governing equations described by eq. (3.20) and thus, it implies that the reaction mass rates of the species are linearly related as

$$\dot{\omega}_f = \frac{1}{r}\,\dot{\omega}_o = -\frac{1}{r+1}\,\dot{\omega}_p\,. \tag{3.23}$$

An Arrhenius-type reaction rate with $r = 1$ is assumed. The source term in the fuel species concentration equation reads

$$\dot{\omega}_f = -\,k_r\,\rho^2\,\theta_o\,\theta_f\,\exp(-Ze/T), \tag{3.24}$$

where $Ze = E_a/RT_j$ is the Zeldovich number and k_r is the reaction rate constant. The exponential term is the Boltzmann factor, which from the kinetic theory can be seen to give the fraction of all collisions that have a greater energy than the activation energy. The pre-exponential factor is the collision frequency, and can be further rewritten with the aid of the non-dimensional Damköhler number as $Da = \frac{h}{U_j}\,k_r\rho_j$, where h is a characteristic length scale. The definition of the Damköhler number will be further explained in the following section.

A further simplified reaction term can be considered, which is a function of the density and reactant concentrations and does not depend on the temperature,

$$\dot{\omega}_f = -\,k_r\,\rho^2\theta_o\theta_f. \tag{3.25}$$

The combustion heat release term, $\dot{\omega}_T$, in the energy equation, eq. (3.16), is related to the species reaction rate terms by

$$\dot{\omega}_T = -\sum_{k=1}^{N} \Delta h_{f,k}^0\,\dot{\omega}_k, \tag{3.26}$$

where $\Delta h_{f,k}^0$ is the formation enthalpy of the k^{th}-species. Due to the linear relation between the different reaction-rate terms, see eq. (3.23), $\dot{\omega}_T$ is formulated as

$$\dot{\omega}_T = \frac{Ce}{(\gamma-1)M_0^2}\,e_0\,\dot{\omega}_p, \tag{3.27}$$

where M_0 is the inlet-based Mach number, Ce is the non-dimensional heat release parameter and e_0 is a characteristic measure of the internal energy, e.

3.3. Key non-dimensional numbers

As observed in the previous section, several non-dimensional numbers appear in the formulation of the governing equations. In this section, these numbers and their relevant importance are briefly discussed.

Reynolds number

The Reynolds number Re is a dimensionless number that gives a measure of the ratio of the inertial to viscous forces and in a general sense, gives an indication for the strength of the turbulence. However, characteristic velocity and length scales should be used to deduce meaningful information. In chemically reacting flows, when a substantial amount of heat is released, the local temperature and density of the fluid significantly vary, which result in a wide range of local Reynolds numbers. It is common to report the cold-flow Reynolds number, with properties of the fluid before the chemical reaction occurs. Here, the inlet Reynolds number is defined as

$$Re = \frac{U_j\, h}{\nu_j}, \tag{3.28}$$

where h is the jet inlet height and the j index is used to denote properties at the inlet jet center.

Mach number

The Mach number M is the speed of an object moving through the air, or any other fluid, divided by the speed of sound in that fluid for the particular physical conditions, including the temperature and pressure. Here, the inlet Mach number is defined as

$$M = \frac{U_j}{a}, \tag{3.29}$$

where $a = \sqrt{\gamma RT}$. In this study, the simulations are performed in subsonic speeds, $M < 1$ and the numerical values are specified for each case.

Prandtl number

The Prandtl number Pr is a dimensionless number that is the ratio of momentum diffusivity or kinematic viscosity to thermal diffusivity and is defined as

$$\mathrm{Pr} = \frac{\nu}{\alpha} = \frac{\mu c_p}{\lambda}, \tag{3.30}$$

where ν is the kinematic viscosity, α is the thermal diffusivity and λ is the thermal conductivity. Note that, contrary to the Reynolds number, the Prandtl number contains no length scale in its definition and is dependent only on the fluid state. Prandtl number is used to relate the momentum to heat transport properties and can be found in property tables for different fluids.

Lewis number

The Lewis number is a dimensionless number defined as the ratio of thermal diffusivity to mass diffusivity and can be expressed as

$$Le_k = \frac{\lambda}{\rho C_p \mathcal{D}_k}, \tag{3.31}$$

where λ is the thermal diffusivity and $\mathcal{D}_k$ is the mass diffusion coefficient.

Schmidt number

The Schmidt number is a dimensionless number defined as the ratio of momentum diffusivity or viscosity and mass diffusivity. The Schmidt number, Sc_k compares momentum and molecular diffusion of the k^{th} species and is defined as

$$Sc_k = \frac{\mu}{\rho \mathcal{D}_k} = \Pr Le_k. \tag{3.32}$$

In this study, the Schmidt number is constant and equal to the Prandtl number for all species, which implies a unity assumption of the Lewis number.

Damköhler number

The Damköhler number Da is a dimensionless number used to relate the chemical reaction time scale to a representative time scale of the flow. Various definitions can be found in the literature for the Damköhler number. The general definition of the Damköhler number is

$$Da = \frac{\tau_{\text{conv}}}{\tau_{\text{react}}} = \frac{h}{U_j} k_r \rho_j. \tag{3.33}$$

The flame structure and combustion regime depend on the chemical characteristic time, τ_{react}. For a fast chemistry (low τ_{react} values and high Damköhler numbers), the flame is very thin. For larger values of the chemical time scale, the flame thickness becomes larger and of the same order as the Kolmogorov length scale, η_k.

Karlowitz number

The Karlowitz number is defined as the ratio of the chemical time scale to the Kolmogorov time scale,

$$Ka = \frac{\tau_{\text{react}}}{\tau_{\text{Kolmogorov}}}. \tag{3.34}$$

For premixed combustion, the interactions between the turbulence and the chemistry can be measured by the Karlowitz number.

Zeldovich number

Activation energy of a chemical reaction is the energy that the reactants must acquire before they can react. In practice, the activation energy is determined experimentally, for each particular reaction. The Zeldovich number, is a non-dimensional measure of the temperature sensitivity of the reaction rate, and

here it is defined in terms of the jet inlet temperature, T_j as

$$Ze = \frac{E_a}{R\,T_j} = \frac{T_a}{T_j}. \tag{3.35}$$

Note that the Zeldovich number may be defined as the product of the temperature rise $\alpha = (T_\infty - T_0)/T_\infty$ and the non-dimensional activation energy $E_a R/T_\infty$, however, for the numerical values of the Zeldovich number, the definition in eq. (3.35) is used throughout this thesis.

Non-dimensional heat release parameter

The non-dimensional heat release parameter, Ce is defined as

$$Ce = \frac{-H^0}{c_p\,T_j}, \tag{3.36}$$

where, $-H^0$ is the heat of reaction for the overall chemical reaction.

3.4. DNS, LES or RANS simulations

There are a number of different ways to solve the governing equations and to deal with the turbulent combustion problems numerically. The Reynolds averaged Navier-Stokes (RANS) approach starts with ensemble averaging the governing equations, in which the Reynolds decomposition is used. The turbulence is described through the turbulent stresses and information is provided about the averaged quantities. Large eddy simulation (LES) is an intermediate tool for computing turbulent flows. In LES, the large scales of turbulent flow are resolved and the small scales of the flow are modeled, using the information obtained from the resolved field, see Popov & Pope (2014). Unlike RANS techniques, LES provides a more realistic and detailed time-resolved data analysis possibility, which gives some knowledge about different structures of turbulent flows. See Fureby (2008), for a recent review of general LES applications in engineering problems and Pitsch (2006) for a review on LES of turbulent reacting flows. Indeed, LES is a very useful tool for turbulent flow computations, in particular, when no reaction is involved and modeling issues are restricted to those of the small scales of turbulence. The most accurate computational tool is the direct numerical simulation (DNS), which solves all the flow equations without making any further assumptions, resolves all the scales from the large integral scales down to the small Kolmogorov scales of the flow and even the fine structures of the flame. In turbulent combustion flows, both the time and space resolution requirements for the DNS are more restrict than what is required for the non-reacting counterpart flows. Thus, it may be very expensive to perform a DNS of real-size problems. For instance, for a reaction with a high Damköhler number, the flame becomes thin and therefore a much finer grid resolution is needed. However, DNS provides detailed information about the different mixing and reaction interactions in the turbulent flow field and thus paves the way for development of new accurate combustion models. DNS data are often used for the validation of combustion models, in addition to that,

thorough fundamental insight of the various aspects of the physical problems can be gained through the careful analysis of the data.

3.5. DNS of turbulent reactive flows

In the past three decades, DNS has become an essential tool to understand and model turbulent combustion. DNS, numerically solves the set of equations describing turbulent flames by resolving all chemical and flow scales (Baritaud *et al.* 1996; Vervisch & Poinsot 1998). Increasing computational resources have facilitated high-resolution simulations and also simulation of more complex phenomena including that of fluid dynamics coupled with reactions using detailed chemistry (Chen 2011; Yu *et al.* 2012; Krisman *et al.* 2014). An example is the reacting flow simulation performed by Knaus & Pantano (2009) to study the heat release effect in shear layers.

DNS investigations are beneficial in mixing and combustion applications, for the fact that they provide access to the complete solution. All length and time scales are resolved and the higher order statistics, such as correlations, probability density functions and dissipation rates can therefore be computed anywhere in the computational domain. Despite the enormous progress in recent years in the availability of computational resources, but due to the computational restrictions, which are still present, DNS studies are mostly dedicated to the canonical flow fields rather than the real engineering applications. However, DNS provides physical insights into the chemistry-turbulence interactions, which in turn will help to improve the combustion models that can handle the engineering-level calculations.

The progress in the application of DNS to study turbulent premixed and non-premixed combustion has been reviewed by Poinsot *et al.* (1996) and Vervisch & Poinsot (1998). The available literature on DNS of reacting flows and rather recent research capabilities of DNS is reviewed by Westbrook *et al.* (2005). A thorough review of DNS of reacting flow may be found in Vervisch (2000) and also in the recent paper by Chen (2011). Here, a detailed review of the recent DNSs of reacting flows will not be given, instead, the related articles will be mentioned in each paper, separately, when they are related to the particular topic under discussion.

3.5.1. *DNS of flame-wall interaction*

Many combustion applications in confined domains contain regions where mixing and reaction take place close to a wall. Thus, better understanding of the wall effects plays an essential role in gaining insight into the full problem.

Most of DNSs of reacting flows have excluded the wall effects. In cases with wall interactions, a closer look at the fundamental statistics seems to be necessary. However, the numerical investigations of wall-bounded reacting flows have often been restricted to the case of turbulent boundary layers and

turbulent channel flows, see Ruetsch *et al.* (1995). A recent example is the work by Gruber *et al.* (2010), who investigated the turbulent flame-wall interaction in a channel flow.

These studies have produced important insights, but much more remains to be studied in the area of wall-bounded turbulent combustion. Poinsot *et al.* (1993) studied the flame-wall interactions of laminar and premixed combustion using compressible two-dimensional DNS with a simple reaction. Bruneaux *et al.* (1996) performed incompressible three-dimensional simulations of premixed combustion in a channel using a simple reaction. They found that quenching distances decrease and maximum heat fluxes increase, in comparison to those of laminar flames. Their DNS data were also used by Bruneaux *et al.* (1997) to develop and evaluate a flame surface density model. Using a complex reaction mechanism, consisting of 18 reactions involving 8 species, one-dimensional premixed and non-premixed flame interaction with an inert wall was simulated by Dabrieau *et al.* (2003). Wang & Trouvé (2006) used DNS to study flame structure and extinction events of non-premixed flames interacting with a cold wall. Their simulation was fully compressible, two-dimensional and the reaction was described using a single-step model containing four species.

3.6. Combustion modeling tools

Modeling of turbulent combustion is a challenging task. In turbulent flames, various difficulties such as strong heat-release, complex chemistry and large ranges of time and length scales are added to the conventional complexities present in constant-density turbulent flows. Thus, both turbulence and combustion models need to be improved and this needs to be done in a meaningful way. The new models are expected to predict much wider ranges of turbulent combustion regimes and, of course, to be more accurate. The understanding and prediction of the behavior of turbulent reacting flows is generally much more difficult than for non-reacting flows. These difficulties arise for different reasons, the most common is the compressibility effects, which make it necessary to solve the conservation of energy equation beside mass and momentum equations. Next, reacting flows in general include heat release and significant density fluctuations and this has implications for the averaging of the governing equations. The mean heat-release rate is one of the main quantities that needs to be approximated in combustion modeling and is often of important practical interest. Moreover, conservation equations for chemical species must be included. Furthermore, turbulent combustion systems involve multiple phases which adds to the complexity of modeling issues, see Veynante & Vervisch (2002), Riley (1998) or Vervisch & Veynante (2011) for an introduction to combustion modeling.

3.6.1. *Premixed and non-premixed combustion modeling*

Two classifications of reactions are generally used in turbulent combustion, which simplify the problem, particularly in development and utilization of models, namely premixed and non-premixed. The two combustion modes were briefly introduced in chapter 2. The former is the reaction between a premixed fuel and oxidant, which are locally ignited by means of a spark, a common example is the internal combustion engine. The ignition starts the flame which propagates through the mixture and generates hot products. In the non-premixed regime, the fuel and oxidizer are introduced separately, for example a fuel jet, which is injected into air. Chemical reaction can occur as the fuel and oxidant mix locally at the molecular level. Therefore, the flame can exist where the fuel and oxidant are mixed locally and the reaction depends on the mixing rate, at least to some extent. Finally, reactions can also occur when the species are partially premixed. For example, in the problem of a fuel jet into air, it is possible for the fuel and air to mix to some extent before the ignition occurs.

If we consider a simplified one-step irreversible premixed chemical reaction,

$$Reactants \quad \longrightarrow \quad Products \quad + \quad Heat, \tag{3.37}$$

we can describe the flame using a *progress variable* c, such that $c = 0$ in the fresh gases and $c = 1$ in the fully burned ones. This progress variable may be defined using the temperature or mass fraction

$$c = \frac{T - T_u}{T_b - T_u} \qquad \text{or} \qquad c = \frac{\theta_f - \theta_f^u}{\theta_f^b - \theta_f^u}. \tag{3.38}$$

Here, T, T_u and T_b are the local temperature, the unburned temperature and the burned gases temperatures respectively; and accordingly θ_f, θ_f^u and θ_f^b are the local, unburned gases and burned gases fuel mass fractions. Assuming the same molecular and thermal diffusivities, unity Lewis number, without heat losses or compressibility effects, then the two definitions are equivalent and mass and energy balance equations reduce to a single balance equation for the progress variable,

$$\frac{\partial \rho\, c}{\partial t} + \frac{\partial}{\partial x_j}\left(\rho\, c\, u_j\right) = \frac{\partial}{\partial x_j}\left(\rho\, \mathcal{D} \frac{\partial c}{\partial x_j}\right) - \dot{\omega}. \tag{3.39}$$

This equation describes the displacement of the $c-$isosurfaces.

For the non-premixed case, we can consider an irreversible one-step chemical reaction as,

$$F \; + \; r\, O \longrightarrow (1 + r)\, P + heat, \tag{3.40}$$

where r is the stoichiometric coefficient. The mixture fraction Z is defined as

$$Z = \frac{\phi\, \frac{\theta_f}{\theta_{f,0}} - \frac{\theta_o}{\theta_{o,0}} + 1}{\phi + 1} \; = \; \frac{r\, \theta_f - \theta_o + \theta_{o,0}}{r\, \theta_{f,0} + \theta_{o,0}}, \tag{3.41}$$

where $\theta_{f,0}$ is the fuel mass fraction in the fuel stream, $\theta_{o,0}$ is the oxidizer mass fraction in the oxidizer stream and ϕ is the equivalence ratio of the non-premixed flame

$$\phi = \frac{r\,\theta_{f,0}}{\theta_{o,0}}. \tag{3.42}$$

The mixture fraction obeys the balance equation,

$$\frac{\partial \rho\, Z}{\partial t} + \frac{\partial}{\partial x_j}\left(\rho\, Z\, u_j\right) = \frac{\partial}{\partial x_j}\left(\rho\, \mathcal{D} \frac{\partial Z}{\partial x_j}\right), \tag{3.43}$$

which does not include a source term. An important value of Z is its stoichiometric value, Z_{st}, which is obtained when fuel and oxidizer are in the stoichiometric condition, i.e. $r\,\theta_f = \theta_o$. Thus the stoichiometric mixture fraction is

$$Z_{st} = \frac{\theta_{o,0}}{r\,\theta_{f,0} + \theta_{o,0}} = \frac{1}{r\,\phi + 1}. \tag{3.44}$$

3.6.2. *Non-premixed combustion modeling tools*

In this section, some basic tools in non-premixed combustion modeling are briefly introduced. Though, nor the modeling in general, neither the non-premixed combustion modeling in particular, are included directly as part of this study, a cursory background is provided here.

The mean heat release rate is one of the main quantities of practical interest that should be approximated by a turbulent combustion model. The simplest and more direct approach is to express the chemical rate in Taylor series as a function of species mass fractions and temperatures. To understand the basic difficulty of applying averaging methods to reacting flows, consider the approximately constant density, one step Arrhenius-type reaction obeying eq. (3.40). Here, one unit of mass of fuel F combines with r units of mass of oxidizer, O to produce $(1+r)$ units of mass of products, P in addition to heat, the fuel reaction rate is approximately given as

$$\dot{w}_F = -k_r\, \rho^2\, \theta_F\, \theta_O\, e^{(-E_a/RT)}. \tag{3.45}$$

Here, k_r is a rate constant, which is commonly called the pre-exponential factor in the Arrhenius expression, T is the fluid temperature and E_a is the activation energy of the reaction, see Riley (1998). Assuming a constant density ρ, the conservation equation (3.39) for the fuel reads

$$\frac{\partial \theta_F}{\partial t} + \frac{\partial}{\partial x_j}\left(u_j\, \theta_F\right) = \frac{\partial}{\partial x_j}\left(\mathcal{D} \frac{\partial \theta_F}{\partial x_j}\right) - \rho\, \theta_F\, \theta_O\, k_r\, e^{(-T_a/T)}, \tag{3.46}$$

where $T_a = E_a/R$ is the activation temperature. Averaging eq. (3.46) gives

$$\frac{\partial \overline{\theta_F}}{\partial t} + \overline{u_j} \frac{\partial \overline{\theta_F}}{\partial x_j} = \frac{\partial}{\partial x_j}\overline{\left(\mathcal{D} \frac{\partial \theta_F}{\partial x_j}\right)} - \frac{\partial}{\partial x_j}\overline{\left(u_j'\, \theta_F'\right)} - \overline{\rho\, \theta_F\, \theta_O\, k_r\, e^{(-T_a/T)}}. \tag{3.47}$$

Two unclosed terms appear after the averaging procedure, one is $\overline{\left(u_j'\theta_F'\right)}$, which is similar to the Reynolds shear stress term in the averaged momentum equations, and can supposedly be modeled in a similar manner. The second term, namely $\overline{\rho\theta_F\theta_O k_r e^{(-T_a/T)}}$, is the average of the reaction rate term, which is the root of the essential difficulties. Often, for example in non-premixed reaction, the flame zone is very thin. Thus, flow consists of regions of either fuel or oxidizer species, with very little overlap and high segregation, i.e. $\overline{\theta_F\,\theta_O} \ll \overline{\theta_F}\;\overline{\theta_O}$. Note that, this type of averaging approach for the cases with $T \approx const.$, is used in chemical engineering problems, however, if $T \neq const.$, one needs to expand the exponents in the form of the Taylor series. Understandably, even for small temperature fluctuations, the modeling will become very difficult. Since accurately modeling the higher order correlations of $1/T$ and the species mass fractions is generally not feasible, other tools are used in turbulent combustion modeling.

3.6.3. *Geometrical approach: flame surface analysis*

In this approach, the flame front is described as a geometrical entity. Here, the analysis is generally linked to the assumption of a sufficiently thin flame, viewed as an interface between fresh and burned gases in premixed combustion or as an interface between fuel and oxidizer in non-premixed cases. Two formalisms are usually proposed within this framework: G-field equation and flame surface density concept.

The G-equation model proposed by Williams (1985), uses an iso-surface method to describe the evolution of the flame front as an interface between the unburned and burned gases. The function G is a scalar field defined such that the flame front position is at $G = G_0$ and that G is negative in the unburned mixture. The instantaneous and local G-equation can be derived by considering the instantaneous flame surface. The details of this method is not discussed any further in the present study.

In the flame surface density description, the flame is identified as a surface and its surface density Σ is introduced. As the flame propagates normal to itself, the mean burning rate is directly proportional to the flame surface area.

3.6.4. *Statistical approach: probability density function*

Prediction of radicals, intermediate species and pollutants requires knowledge of the flame internal structure, for the intermediate states between fresh and burned gases in premixed flames or between fuel and oxidizer in non-premixed flames. Despite the fact that, in the G-field equation or in the flame surface density approaches, some statistical treatment is performed, but they are based on the geometrical view of the flame as a thin interface. In probability density function (PDF) methods, this assumption is relaxed and one can focus on the statistical characteristics of the flame, throughout intermediate states of the flame and different regions of the flow, see O'Brien (1980), Pope (1985) and Dopazo (1994).

Considering a non-premixed flame, where the chemistry is reduced to a single-step reaction and the radiative heat losses are neglected, laminar combustion may be parameterized with two variables, for instance, fuel mass fraction, θ_F and mixture fraction Z. The turbulent flame is then fully described by the joint PDF of mixture fraction and fuel mass fraction, $\overline{P}(\theta_f, Z; x, t)$. For such flames, it is interesting to focus on the statistical properties of the fuel mass fraction, θ_f for a given value of the mixture fraction Z. According to Vervisch & Veynante (2011), two main directions may be chosen to build numerical models from PDF. One is to presume the PDF shape from the available mean quantities and the other is to solve a balance equation for the PDF.

3.6.5. *Mixture fraction approach: small scales analysis*

Turbulent mixing can be used as a measure for quantifying the burning rate. In case of a large Damköhler number, which is a common assumption in combustion modeling, the reaction rate is limited by turbulent mixing and it may be described in terms of the scalar dissipation rate. Peters (2000) defines flamelets as "thin diffusion layers embedded in a turbulent non-reactive flow field". This thin region is assumed to be smaller than the Kolmogorov length scale and therefore it is locally laminar. The flame surface is defined as an iso-surface of the mixture fraction, Z in non-premixed combustion. In non-premixed flames, fresh fuel and oxidizer need to be mixed at the molecular level for reaction to take place and the flame is mainly controlled by turbulent mixing occurring between the two gas streams. If we assume equal molecular diffusivities for all chemical species, the mixture fraction, Z can be defined as the local mass fraction of a conserved scalar originating in the fuel stream. In the case of infinite rate or equilibrium chemistry, the concentrations of the various chemical species can be functionally related to the mixture fraction, enabling the average concentrations to be expressed in terms of these relationships and the probability density of the mixture fraction. For finite-rate chemistry, theories have been developed relating the average concentrations to the joint probability density of Z and its dissipation rate χ. The scalar dissipation rate, χ provides a direct measure for the decay rate of the fluctuations (Veynante & Vervisch 2002).

3.6.6. *Non-premixed combustion modeling issues*

In previous sections, the major important tools, which are used in turbulent combustion modeling were briefly introduced. The three most useful quantities for description of a turbulent flame were introduced, namely, the scalar dissipation rate, the probability density functions and the flame surface density. A schematic of the different types of modeling tools for non-premixed combustion is presented in figure 3.1[3]. Interestingly, all these quantities are interrelated and the links between them have been developed. The exact relation between

[3]This figure is originally generated by the author for the purpose of present work, however, it has the spirit of a similar figure in the paper by Vervisch (2000).

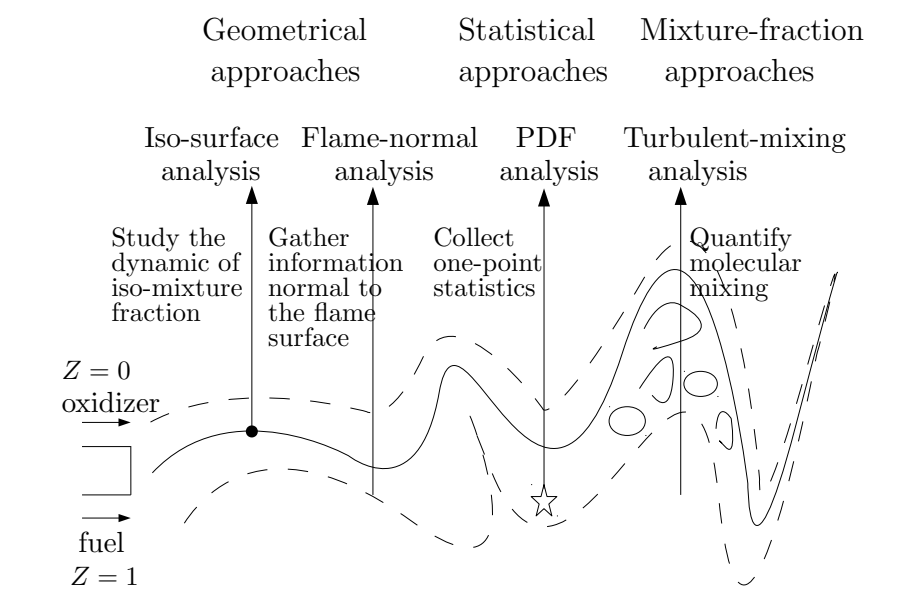

FIGURE 3.1. Schematic of different combustion modeling approaches

the mean scalar dissipation rate, probability density function and the generalized flame surface density can be found in Veynante & Vervisch (2002). These relations show that the scalar dissipation rate is a key quantity that directly or indirectly relates different tools to each other. Thus, studying its behavior throughout the simulation field is of prominent importance. Having access to the full range of scales, provided by DNS data analysis, it can be focused on the characteristics of these essential quantities everywhere in the domain, including their near-wall behavior.

3.7. Subgrid-scale modeling in turbulent reacting flows

DNS databases are often used to evaluate subgrid-scale (SGS) models and statistics in LES using *a priori* analysis. Due to compressibility effects, existence of source terms in the governing equations of the scalar species and many other complexities, SGS modeling is more complicated in turbulent reacting flows than in incompressible non-reacting ones.

In LES, a separation of scales is performed by filtering, for instance, the velocity and scalar fields. The filtering in LES is commonly defined as (Leonard 1974)

$$\underline{\phi}(x,t) = \int_D G(x-x')\phi(x',t)ix', \tag{3.48}$$

where $\underline{\phi}(x,t)$ is the filtered quantity, $\phi(x,t)$ is the variable to be filtered, G is the kernel of the convolution and D is the domain of integration. A differential

form of the filter (3.48) can be obtained by a Taylor series expansion of G in powers of the filter size as

$$\underline{\phi}(x,t) = \sum_{k=0}^{\infty} \frac{1}{k!} \mathcal{M}_k \frac{\partial^k \phi(x,t)}{\partial x^k}, \tag{3.49}$$

where M_k are the moments of the filter kernel

$$\mathcal{M}_k = \int_D x^k G(x) dx. \tag{3.50}$$

Different types of filters can be written using this formulation, for instance, the box filter can be written in the differential form as Sagaut (2000)

$$\underline{\phi}(x,t) = \phi(x,t) + \frac{\underline{\Delta}^2}{24} \frac{\partial^2 \phi(x,t)}{\partial x^2} + \frac{\underline{\Delta}^4}{1920} \frac{\partial^4 \phi(x,t)}{\partial x^4}. \tag{3.51}$$

CHAPTER 4

Turbulent wall-jet flame

4.1. Wall-jet set-up and background

A wide range of flows have been described with the "wall-jet" terminology, all sharing a common characteristic, that the outer part of these flows behaves similar to a jet flow and the inner part behaves more or less like a boundary layer flow. A wall-jet is formed, when a jet flow evolves over a flat surface in the absence or presence of an external stream. Depending on the type of the jet, its injection direction, the nozzle geometry and wall boundary conditions, such as the surface temperature or roughness, many different kinds of wall-jet flows may form. A few examples are, two-dimensional planar wall-jets, studied by Conlon & Lichter (1995), the coflow wall-jets, Coanda wall-jets (wall-jets on curved surfaces), investigated by Neuendorf & Wygnanski (1999), three-dimensional wall-jets addressed by Hall & Ewing (2010) and different kinds of impinging jets.

The turbulent wall-jet includes a number of interesting fluid mechanics phenomena with a close resemblance to many engineering applications. Wall-jets are widely used for boundary layer control, cooling of turbine blades, and to enhance or reduce the convective wall heat-transfer. Impinging wall-jets have applications in heating or annealing of metal, plastic or glass during the manufacturing process, where this technique is used to control the processing temperature. Wall-jets are also formed when fuel is injected into internal combustion engines. Sometimes, wall-jets are injected parallel to the inner surface of a combustion chamber to protect it from the hot products. In supersonic aeronautical applications, wall-jet flow occurs when fuel is injected into the boundary layer for drag reduction purposes.

The "wall-jet" flow was addressed by Glauert (1956), where the term was initially used. Though, this was not the first work on wall-jets, but perhaps the first one dedicated to the subject. One of the earliest known works on wall-jets is an experimental study by Förthmann (1934), in which he extended his research on jet flows to jets close to a surface. Since the 60's, numerous experimental, theoretical and also some numerical studies have been performed on different kinds of wall-jets. A comprehensive review on the turbulent wall-jet experiments prior to 1980 can be found in Launder & Rodi (1981), a few of which are mentioned below. Förthmann (1934) observed the self-preserving nature of the wall-jet, and that the boundary-layer thickness varies linearly

with downstream position, x, and that the maximum velocity varies as $x^{-1/2}$. Glauert (1956) was maybe the first to divide the flow into an inner and outer part on either side of the maximum velocity and treated the two regions separately. In many studies, particular attention has been paid to the appropriate similarities in different regions of the wall-jet flow and the corresponding velocity and length scales. Narashima *et al.* (1973) suggested that the mean flow parameters should scale with the jet momentum flux and the kinematic viscosity. The same approach was employed by Wygnanski *et al.* (1992) to remove inlet Reynolds number dependency and to determine the skin friction from the decrease in the momentum flux; see also Zhou *et al.* (1996). George *et al.* (2000) performed a similarity analysis of the inner and outer part of the wall-jet without a coflow, using different experimental data of previous studies. Parallel to the analytical works on the similarity characteristics of the wall-jet flow, experimental work was initiated by Bradshaw & Gee (1960). They performed measurements of a turbulent wall-jet and reported that the turbulent shear stress attains a finite value at the point of maximum velocity. Eriksson *et al.* (1998) studied a wall-jet in a large water tank using Laser Doppler Velocimetry for their measurements. A rather recent experimental study on plane wall jets was reported by Dey *et al.* (2010) in which, they investigated the effects of suction and injection from the wall.

Although experimental and theoretical studies on the wall-jet flows have been numerous in the past, the numerical research has remained limited. Accurate numerical data can indeed, strengthen conclusions on scaling and similarity and also provide a closer insight into the development of the jet, including the transitional features. However, performing a numerical simulation of the spatially developing turbulent wall-jet flow is computationally expensive, thus, reports on simulations of the wall-jet flow are scarce. The very early computational studies of the plane turbulent wall-jet, using Reynolds averaged Navier-Stokes (RANS) modeling, are given in the review by Launder & Rodi (1981). Dejoan & Leschziner (2005) performed a well-resolved large eddy simulation and compared the results with the experiments by Eriksson *et al.* (1998). The results agreed well with the experiments for the velocities and Reynolds stresses. Wernz & Fasel (1996, 1997) employed DNS to investigate instability mechanisms in a transitional wall-jet. The breakdown of a finite-aspect-ratio wall-jet was studied by Visbal *et al.* (1998). Levin *et al.* (2005) studied the laminar breakdown of a wall-jet using linear stability analysis and DNS. Gogineni *et al.* (1999) studied transitional two-dimensional wall-jets at a low Reynolds number. DNSs of isothermal and non-isothermal non-reacting turbulent wall-jet flows were performed by Ahlman *et al.* (2007, 2009). DNS of isothermal and exothermic chemically reacting turbulent wall-jets were performed by Pouransari *et al.* (2011, 2013).

A schematic of the plane turbulent wall-jet geometry is shown in figure 4.1, where h is the jet inlet height and the x and y axes denote dimensions in the streamwise and wall-normal directions, respectively, and the spanwise direction

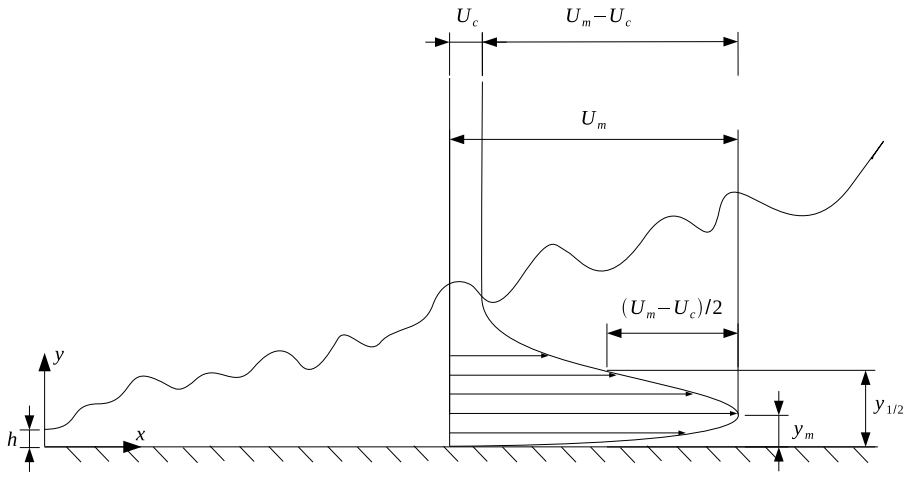

FIGURE 4.1. Schematic of the plane turbulent wall-jet with coflow. Figure taken from Pouransari *et al.* (2015*a*).

is perpendicular to this plane. Here, U_m is the local maximum velocity and U_c is the coflow velocity. For the plane wall-jet with coflow, the velocity half-height $y_{1/2}$ is defined as the distance from the wall to the position where the mean velocity is half of the maximum excess value, $U(y_{1/2}) = \frac{1}{2}(U_m - U_c) + U_c$[1].

The structure of a developed turbulent wall-jet can formally be described as two adjacent shear layers of different character. The inner layer, extending from the wall up to the maximum mean streamwise velocity, resembles a thin boundary layer, while the outer part, positioned above the inner layer and reaching out to the ambient flow, can be characterized as a free shear flow. However, there are certain distinctions between the inner layer of wall-jet flows and boundary layer flows. One difference is the intermittent nature of the outer part of the turbulent boundary layer. Another point of difference lies in the modification of the structure of the inner layer of the wall-jet by the turbulence in the outer layer. Furthermore, the skin-friction coefficient of a turbulent boundary layer varies in a different manner from that of the wall-jet. These factors prevent a complete analogy between the inner layer of the wall-jet and the turbulent boundary layer. Considering these restrictions, Hogg *et al.* (1997) concluded that the initial streamwise momentum flux and the kinematic viscosity are suitable parameters governing the flow evolution.

The wall-jet flow is a suitable configuration for examining the interactions between the outer and inner structures in a turbulent boundary layer. The interactions present in the turbulent plane wall-jet configuration are, in particular, of great interest for the reaction and mixing applications. The turbulent

[1]This formulation is by mistake mistyped as $U(y_{1/2}) = \frac{1}{2}(U_m - U_c)$ in papers 1, 2, 3 and 6, but, it is correctly expressed in paper 4 and 5. However, the figures and numerical values are correct in all papers.

wall-jet is much more flexible and controllable than the boundary layer. Adding an external coflow to the wall-jet setup increases the parametric flexibility even further, for instance, changing the ratio between the free stream velocity and the jet velocity, leads to formation of different flow fields. Understanding the turbulence structures and physical dynamics of the problem is, however, crucial for analyzing mixing, heat transfer, drag reduction and other phenomena, which occur in turbulent wall-jet flows.

4.1.1. *Scalings for compressible turbulent wall-jet*

There is a general agreement that the mean velocity profile of the turbulent wall-jet is self-similar, but the scaling parameters are controversial among different researchers. In this section, a brief introduction to the most commonly used scaling parameters for compressible turbulent plane wall-jet flow is presented. Even though, the present study is not focused on the similarities in the inner and outer regions of the wall-jet flow, the requisite search for the proper scales have been performed and the choice of velocity and length scales for each region is discussed.

If we hypothesize that the inner part of the wall-jet and zero-pressure-gradient boundary layers are similar, it would be appropriate to use the same scaling here as well. However, the interaction of large turbulence scales in the outer layer with small scales in the inner layer substantially affects the development of the wall-jet.

4.1.1.1. *Inner layer scaling*

The inner-layer scaling for the boundary layer flows was introduced by Prandtl (1932), where appropriate inner length and velocity scales were defined as:

$$l = \frac{\nu}{u_\tau}, \tag{4.1}$$

$$u_\tau^2 = \frac{\tau_w}{\rho}, \tag{4.2}$$

where $\tau_w = \rho\,\nu\,(\frac{\partial U}{\partial y})_{y=0}$ is the wall shear stress and y is the distance from the wall. Performing dimensional analysis in the near-wall region, assuming that the outer effects are negligible, we can acquire universal functions, f and g, for the velocity and Reynolds shear stress as,

$$U^+ = \frac{U}{u_\tau} = f(y^+), \tag{4.3}$$

$$-\overline{uv}^+ = \frac{-\overline{uv}}{u_\tau^2} = g(y^+), \tag{4.4}$$

where $y^+ = y/l$. Relation (4.3) is called *the law of the wall*. A vast number of experimental, analytical, and numerical investigations in wall-bounded flows, including channel, pipe and boundary layer flows have been performed to show that the function $f(y^+)$ has a universal form. At the wall, the no-slip condition corresponds to $f(0) = 0$. A Taylor series expansion for small y^+ shows that

the linear relation $U^+ = y^+$ is a good approximation in the near-wall region. Simulations and experimental studies of wall-bounded flows show that the linear relation (4.3) is valid for approximately $y^+ < 5$.

4.1.1.2. *Outer layer scaling*

Assuming similar characteristics to that of the plane turbulent jet in the outer layer, the appropriate outer length and velocity scales are defined as,

$$l_{outer} = y_{1/2}, \tag{4.5}$$

$$U_{outer} = U_m. \tag{4.6}$$

The velocity half-height, $y_{1/2}$ was defined as the distance from the wall to the position with a mean velocity of half of the excess value, $U(y_{1/2}) = \frac{1}{2}(U_m - U_c) + U_c$.

The friction Reynolds number, Re_τ is defined as

$$Re_\tau = \frac{\delta}{l} = \frac{u_\tau \delta}{\nu_w} = \frac{\delta}{\nu_w^{1/2}} \sqrt{\left(\frac{\partial U}{\partial y}\right)_{y=0}}, \tag{4.7}$$

where ν_w is the kinematic viscosity at the wall. When an appropriate outer length-scale δ is used, the friction Reynolds number can be seen as an estimate of the outer-layer to inner-layer length-scale ratio. Throughout this study, the half-height of the jet is used as the outer length scale.

4.1.2. *Semi-local scaling*

To include a measure for the velocity fluctuations rather than the absolute values of the Favre averaged fluctuation intensities, one approach is to account for the varying mean density by using the semi-local scaling. In this scaling the wall variables are based on the local mean density and viscosity, and their relation to the conventional wall units are

$$u_\tau^* = \sqrt{\frac{\tau_w}{\bar{\rho}}} = \sqrt{\frac{\bar{\rho}_w}{\bar{\rho}}} u_\tau, \tag{4.8}$$

$$l^* = \frac{\bar{\nu}}{u_\tau^*} = \frac{\bar{\nu}}{\nu_w} \sqrt{\frac{\bar{\rho}}{\rho_w}}\, l. \tag{4.9}$$

The corresponding normalized wall distance becomes

$$y^* = \frac{y}{l^*}. \tag{4.10}$$

4.2. DNS of reacting turbulent wall-jets

4.2.1. *The DNS code*

The simulation code was originally provided by Prof. B. J. Boersma, and has been used to study a turbulent round jet flow, see Boersma (2004).

The DNS code was further developed for a wall-jet configuration by Ahlman (2007). The main changes included the implementation of boundary conditions

of the computational domain, for instance, at the wall a no-flux condition was prescribed. Moreover, for the simulations of isothermal and non-isothermal turbulent wall-jets, suitable target functions for the density and energy at the outlet were developed.

In the present study, to simulate the exothermic reacting turbulent wall-jets, Arrhenius-type expressions for the source terms of the two additional scalar transport equations, describing the oxidizer and fuel mass fractions, were implemented and the energy equation was modified accordingly to account for the combustion heat release.

4.2.2. *Numerical method and parameters*

The numerical method used in the simulations employs a 6^{th} order compact finite difference scheme and a 4^{th} order Runge-Kutta method for the spatial and temporal integration, respectively, of the fully compressible mass, momentum and energy conservation equations, eqs. (3.1), (3.4) and (3.16).

The turbulent wall-jet flow contains a broad range of velocity and length scales and for a simulation to extend to the self-similar region, a rather large domain is required. Thus, the domain size is chosen such that it is sufficient for the spatial development of the jet and there is enough room after transition, for study of the turbulent wall-jet flow. The computational domain is a rectangular box, the size of which in terms of inlet jet height, h, is $(L_x = 35h)\times(L_y = 17h)\times(L_z = 7.2h)$ in most of the papers, where x, y and z denote the streamwise, wall-normal and spanwise directions, respectively. However, in papers 4 and 5, simulations in a larger box, in particular with a considerably longer axial direction are performed, $(L_x = 48h)\times(L_y = 23h)\times(L_z = 9.6h)$. The number of grid points in each direction are chosen such that there is a fine resolution for a well-resolved DNS in each case. In the streamwise direction, grid stretching is chosen with a higher resolution in the transition region. For instance, in the isothermal simulation in Pouransari *et al.* (2013), at the downstream position $x/h = 25$, where most of the statistics shown in the following sections are taken, the streamwise resolution is about $\Delta x^+ \approx 10$, and the spanwise resolution is about $\Delta z^+ \approx 6$, expressed in wall units. In the wall-normal direction, the grid is finer near the wall to provide sufficient resolution for resolving the inner layer structures. For instance, twelve nodes exist in the near-wall region, below $y^+ = 11$. The Kolmogorov length scale grows with increase in the heat-release, thus, when it comes to the turbulence structures, using similar grids for the isothermal and exothermic cases means a finer resolution for the exothermic one. This is addressed and discussed in Pouransari *et al.* (2015*a*).

The inlet based Reynolds and Mach numbers of the wall-jet flow are defined by eqs. (3.28) and (3.29), respectively and the compressibility effects are found to be small. Their numerical values are $Re = 2000$ and $M = 0.5$ in most of simulations, while in paper 6, $Re = 6000$. For the heat fluxes, a constant Prandtl number $Pr = \mu c_p/\lambda = 0.72$ is used. The Schmidt number of the

scalars, defined with eq. (3.32), is constant and equal to the Prandtl number, $Sc = 0.72$.

At the wall, the no-slip condition is fulfilled for the velocity and a no-flux condition, $(\frac{\partial \theta}{\partial y})_{y=0} = 0$, is applied for the scalars. Periodic boundary conditions are used in the spanwise direction. The ambient flow above the jet has a constant coflow velocity of $U_c = 0.10\,U_j$, where U_j is the jet inlet velocity. At the top of the domain, an inflow velocity of $0.026\,U_j$ is used to account for the entrainment. To prevent the reflection and generation of waves, sponge zones are implemented at the inlet and outlet boundaries.

A single-step irreversible reaction as described in eq. (3.22) is used. In the isothermal reacting wall jet cases, a simplified reaction term is considered, which is a function of density and reactant concentrations and does not depend on temperature, as in eq. (3.25). In the exothermic reacting simulations, an Arrhenius-type reaction rate, according to eq. (3.24), is considered. However, parameters are chosen in a way that the simulations have comparable rates of fuel consumption throughout the domain. In the isothermal cases, the reaction is temperature independent and does not release heat. The flow is uncoupled from the chemical reaction and the influence of the turbulent mixing on the reaction can be studied in the absence of temperature effects. In the exothermic cases instead, the heat-release effects on the turbulence structures can be examined.

The reacting scalars enter the domain separately in a non-premixed manner. At the jet inlet $\theta_{f,j} = 1$ (pure fuel), while in the coflow $\theta_{o,c} = 0.5$ (air enriched at 50% oxygen in mass). Here, $\theta_{f,j}$ is the fuel mass fraction in the fuel stream (the jet flow), and $\theta_{o,c}$ is the oxidizer mass fraction in the oxidizer stream (the coflow). Thus, using equation (3.42) for calculating ϕ, the equivalence ratio of the non-premixed flame for the present mixture, the value $\phi = \theta_{f,j}/\theta_{o,c} = 2$ is obtained and using the succeeding relation, eq. (3.44), the value of the stoichiometric mixture fraction is $Z_{st} = 0.33$. Apart from the reactants, an additional passive scalar equation, injected through the jet stream, is solved for comparison, which also serves as a representative of the local mixture fraction.

For details of numerical implementations, including the boundary conditions, the grid generation, and also the issues concerning the high wave number disturbances, treatment of occurrences of negative concentrations and the transition to turbulence, see the work by Ahlman (2007). However, the relevant matters for each paper are addressed therein accordingly.

4.2.3. *Development of the turbulent wall-jet flame*

In this section, some of the key statistics and visualizations of the reacting turbulent wall-jet flow are presented. Presenting some of the results for the isothermal and exothermic reacting wall-jets has a two-fold ground, one is to provide an introduction to the dynamics of a reacting turbulent wall-jet and

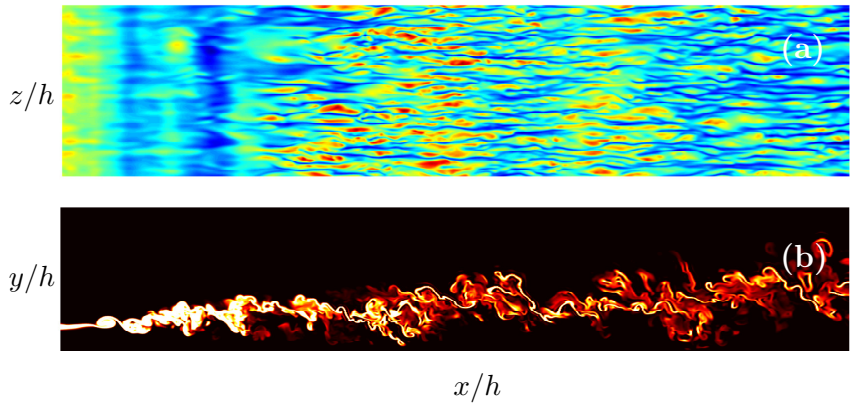

FIGURE 4.2. Instantaneous snapshots of (a) the streamwise velocity fluctuations at a fixed $xz-$plane; $8 < y^+ < 10$; Red and blue colors represent positive and negative fluctuations, respectively, and (b) the reaction rate fields for a fixed $xy-$plane; The lighter color indicates a higher reaction rate. Figure produced from the DNS data of Pouransari *et al.* (2014)

the other is to give a valuable material to illustrate the primary effects of the heat release.

To provide an overview of the turbulence structures and the temperature rise of the flow field in the turbulent wall-jet simulation, instantaneous snapshots of the streamwise velocity and temperature fields for one of the exothermic cases in Pouransari *et al.* (2013) are visualized in figures 1.1 (a) and (b). The flow is from left to right and is evolving in space. The streamwise velocity is scaled with the jet inlet velocity and temperatures are given in Kelvin. Visualizations of the instantaneous fields show that the jet is fully turbulent in half of the domain.

Figure 4.2 (a) shows instantaneous fluctuations of the streamwise velocity in the $xz-$plane at $y^+ \approx 9$ for the isothermal reacting case with the inlet based Reynolds number of $Re = 6000$, presented in Pouransari *et al.* (2014). The typical near-wall elongated streaky structures, similar to other turbulent wall-bounded flows, are clearly observed in the streamwise velocity fluctuations. Figure 4.2 (b) shows a snapshot of the instantaneous reaction rate for the same case. The reaction starts immediately after the inlet and spreads as the flow evolves in the downstream direction. The reaction occurs mainly in the upper shear layer in thin sheet-like structures, however, reactions also take place near the wall, although to a lesser extent. The flame is wrinkled, folded and convoluted in different regions. In the near-wall region, turbulent patches of high concentrations of oxidizer are pumped toward the wall, which result in the formation of spots of high reaction rates close to the wall.

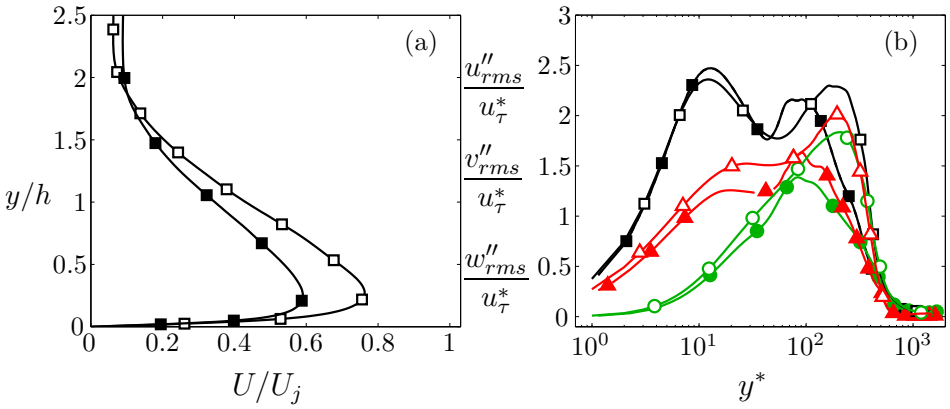

FIGURE 4.3. Cross-stream profiles of (a) mean streamwise velocity, —□— : isothermal, —■— : exothermic, taken from a figure in Pouransari *et al.* (2015*a*), and (b) streamwise, wall-normal and spanwise velocity fluctuation intensities using semi-local normalization. —□— : Streamwise fluctuations: isothermal, u''_{rms}/u^*_τ, —■— : streamwise fluctuations: exothermic. —○— : wall-normal fluctuations: isothermal, v''_{rms}/u^*_τ; — ● — : wall-normal fluctuations: exothermic. —△— : spanwise fluctuations: isothermal, w'_{rms}/u^*_τ; —▲— : spanwise fluctuations: exothermic. Profiles are at the downstream position $x/h = 25$ and taken from a figure in Pouransari *et al.* (2013).

The cross-stream profiles of the mean streamwise velocity are shown in figure 4.3 (a) for the isothermal and exothermic reacting cases, which illustrate the resulting acceleration of the flow for the exothermic case. The increase in the maximum excess value, i.e. $(U_m - U_c)$, is about 40% for this case at $x/h = 25$, compared to the corresponding isothermal case.

The cross-stream profiles of the three components of the Favre-averaged turbulence intensity for chemically reacting wall-jets are plotted in figure 4.3 (b) using semi-local inner scaling. Using this scaling, it has been attempted to account for the variation of the mean density in the wall-normal direction. See eqs. (4.8) and (4.9) in the previous section. It can be seen from figure 4.3 (b) that the semi-local scaling gives a reasonably good collapse in the inner region, up to $y^+ = 30 - 50$, for all the three intensities. This collapse is substantially better than with the conventional inner scaling.

It is interesting to note the two-peak character of the streamwise turbulence intensity. The magnitude of the outer peak, caused by production of turbulence in the outer shear layer, is of about the same magnitude as the inner peak. The wall-normal fluctuation intensity in a turbulent wall-jet has only one peak, which is roughly the same as the magnitude of the streamwise and spanwise

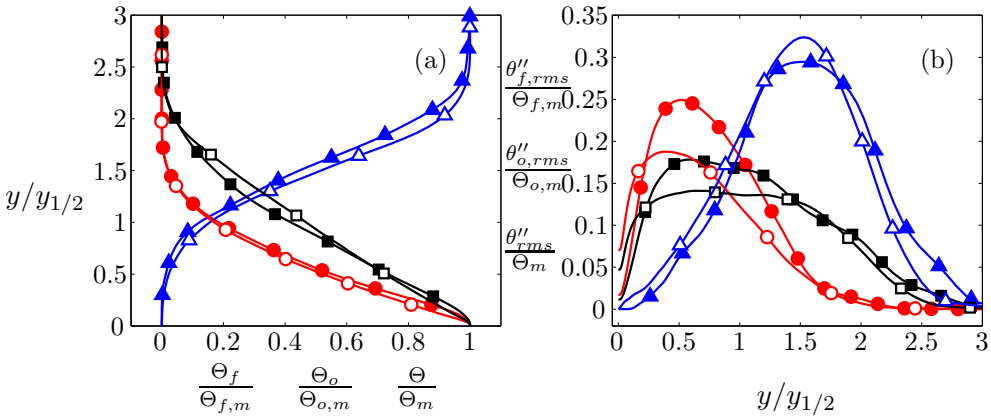

FIGURE 4.4. Statistics of oxidizer (blue), fuel (red) and passive (black) scalars for different cases, (a) cross-stream profiles and (b) fluctuation intensity of the passive and reacting scalars; —□— : Passive scalar isothermal; —■— : passive scalar exothermic; —○— : fuel isothermal; —●— : fuel exothermic. —△— : oxidizer isothermal; —▲— : oxidizer exothermic. Profiles are at the downstream position $x/h = 25$ and taken from a figure in Pouransari *et al.* (2013).

outer peaks. The variation with the heat-release for the outer peak is rather weak. In terms of y^*, positions of the outer maxima for all the quantities in figure 4.3 (b) move closer to the wall with increase of the heat-release.

The cross-stream profiles of the scalar concentrations are displayed in figure 4.4 (a). This plot confirms that all non-reacting and reacting mean scalar profiles for different cases collapse fairly well when outer scaling is used. It is also noticeable that beyond $y/y_{1/2} = 2$, the concentrations of both the conserved scalar and fuel species are very low, therefore, in many of the profiles, shown later in this work, the focus is on the regions where the concentrations are reasonably high, i.e. below $y/y_{1/2} = 3$.

Worth to notice is that, as seen in figure 4.4 (b), the fluctuation level of the reacting scalars has started to decrease around the half-width position, where the reaction is very intense. The peak of the scalar fluctuation intensity increases as a result of the chemical reaction and is further intensified by the heat-release. The increase in the fuel species fluctuation intensity is substantial and the level is about 20%. The oxidizer fluctuation level seems to be less sensitive to the heat-release effects. The wall-normal fluxes exhibit a similar behavior, with increased wall-normal fuel fluxes in accordance with the heat-release-generated increase in the fuel concentration fluctuation intensities.

As discussed briefly in chapter 2, probability density function (PDF) is a practical tool that is often used in the study of velocity and scalar fields in

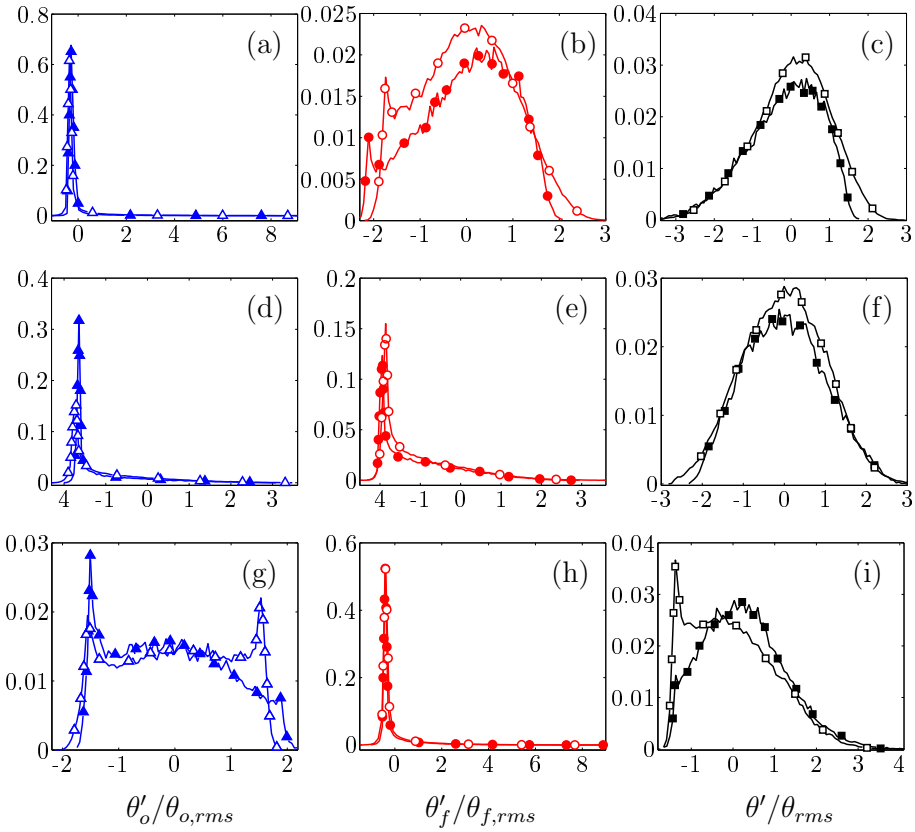

FIGURE 4.5. Probability density functions of different species at three wall-normal locations for both the isothermal and exothermic cases, taken from Pouransari *et al.* (2011) and Pouransari *et al.* (2013), respectively. First row: $y/y_{1/2} = 0.5$, second row: $y/y_{1/2} = 1.0$ and third row: $y/y_{1/2} = 1.5$, where $y_{1/2}$ is the local half-height of the wall-jet in each case at downstream position $x/h = 25$. —□— : Passive scalar isothermal; —■— : passive scalar exothermic; —○— : fuel isothermal; —●— : fuel exothermic. —△— : oxidizer isothermal; —▲— : oxidizer exothermic.

turbulent reacting flows. The shape of the scalar PDFs in the subgrid-scale range in large eddy simulation is indeed a common input to non-premixed combustion models that are prescribed in advance, see the works by Vervisch *et al.* (1995), Cook *et al.* (1997) and de Bruyn-Kops *et al.* (1998).

Figures 4.5 (a-i) show the PDF of the three species, namely oxidizer, fuel and passive scalar for both the isothermal and exothermic reacting cases at $x/h = 25$. Statistics are taken from Pouransari *et al.* (2011) and Pouransari

et al. (2013), respectively. In the fully turbulent region, the PDFs of the species are rather similar, therefore, only one downstream position is shown.

It is interesting to compare the evolution of the fuel concentration with that of the passive scalar simultaneously for the two cases, starting from the wall moving further up to the jet region. As observed in figure 4.5, the PDFs of the fuel and the passive scalar are rather similar from the wall up to the vicinity of the half-height of the jet, $y/y_{1/2} = 1$ plane, but beyond this position the passive scalar PDF still keeps its near-Gaussian shape while the fuel PDF has a large peak at low concentrations showing that much of the fuel has been consumed and deviate significantly from the Gaussian distribution and exhibit long exponential tails in the outer shear layer, which is an indication of the existence of high intermittency, due to the chemical reaction. The presence of an exponential tails can be of particular importance for combustion modeling applications (Vervisch *et al.* 1995; Warhaft 2000; Wall *et al.* 2000; Pouransari *et al.* 2012). In contrast, the passive scalar exhibits a rather symmetric PDF in most of the domain.

The qualitative shape of oxidizer PDFs are similar for the two cases. There is one peak at the minimum concentration, which disappears around $y/y_{1/2} = 2$. Moving away from the wall, the PDF profile are broader around $y/y_{1/2} = 1.5$ and a second peak occurs in the PDF of the oxidizer, which is close to the maximum concentration. This implies that the probability of particles with low concentrations coming from the wall region or caused by reaction with the fuel and particles with high concentrations coming from outer region are both high at this position. However, outside of the jet at about $y/y_{1/2} = 1.5$, as seen in figure 4.5 (g), the probability of observing fluid parcels with higher values of oxidizer fluctuations is higher for the isothermal case compared to the exothermic case. This can be connected to the fact that the heat release has a damping effect on the fluctuation intensity of the oxidizer in this region as seen in figure 4.4 (b), contrary to the other two scalars. Worth to notice is that the shape of the fuel and oxidizer PDF curves are most similar at the half-height planes at any downstream position.

CHAPTER 5

The effects of heat release

The combustion heat release $\dot{\omega}_T$, as it appeared in eq. (3.16), is a source term in the energy equation due to the exothermic chemical reaction, which is related to the species reaction rates, see eq. (3.26). Heat-release modifies the turbulent flow field dynamics in several ways. One is its effect on the turbulence structures that can also influence the turbulent mixing. Due to their importance, heat release effects have been the subjects of a number of different studies (McMurtry *et al.* 1989; Ruetsch *et al.* 1995; Livescu *et al.* 2002; Mizobuchi *et al.* 2005; Diez & Dahm 2007; Knaus & Pantano 2009). These studies are mainly focused on the heat-release effects on the large-scale turbulence structures, energy exchange mechanisms and turbulence spectra. Mostly, mixing layers or free jet flows have been the test case in these studies. Neglecting the presence of the wall, for example in reacting turbulent shear layers, some of the previous studies suggested that, after an appropriate scaling, the effect of heat release on the turbulence is rather small. However, studies on the effects of the combustion heat release on the small scales of turbulence are limited and need to be further explored. Moreover, the heat release effects can also be studied on the scalar fields that are embedded in the turbulent flow.

The present study focuses on the heat release effects in the reacting turbulent wall-jet configuration, which includes the wall effects. In this flow, heat release effects delay the transition, enlarge the fluctuation intensities of density and pressure and also enhance the fluctuation level of the species concentrations. Heat release has a damping effect on all velocity fluctuation intensities and the Reynolds shear stress. Some of the initial heat release effects on basic statistics of the reacting turbulent wall-jet flow were already visualized in chapter 4. In this chapter, we introduce the heat release effects on the flow and flame structures with more details.

5.1. Heat release effects on the turbulence scales

To visualize the heat release effects on the flow dynamics, turbulent structures are plotted using the Q-criterion. The Q-criterion, developed by Hunt, Wray & Moin (1988), is used to extract the zone of intense vortical structures, and is defined through

$$Q = \frac{1}{2}\left(\Omega_{ij}\Omega_{ij} - S_{ij}S_{ij}\right), \tag{5.1}$$

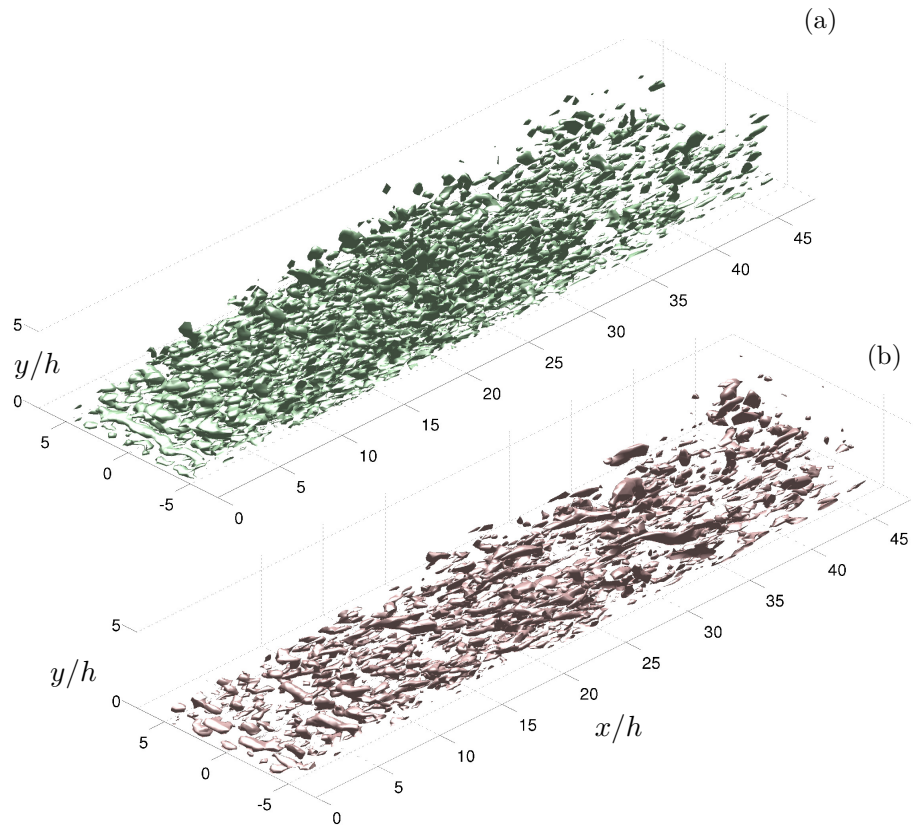

FIGURE 5.1. Iso-surfaces of Q-criterion with $Q_{iso} = 0.1\,(U_j/h)^2$ for (a) isothermal and (b) exothermic cases. Figure is taken from Pouransari *et al.* (2015*c*).

where $S_{ij} = 0.5(\partial u_i/\partial x_j + \partial u_j/\partial x_i)$ and $\Omega_{ij} = 0.5(\partial u_i/\partial x_j - \partial u_j/\partial x_i)$ are the symmetric and antisymmetric parts of the velocity gradient tensor, respectively. Positive values of Q display regions where rotation dominates over the straining. The iso-Q surfaces, representing the normalized second invariant of the velocity gradient tensor are visualized in figure 5.1(a-b) for the isothermal and exothermic cases. Comparison shows that the small-scale vortical structures, present in the isothermal reacting case, have substantially been damped and perhaps merged to larger coherent structures in the exothermic case.

Heat release influences on turbulence scales can be illustrated by examining the premultiplied spectra, which gives a more comprehensive insight into the scale variation throughout the wall-normal axis, see e.g. del Álamo & Jiménez (2003). The premultiplied spectra of the streamwise velocity fluctuations in the spanwise direction are shown in figure 5.2 using the semi-local inner scaling, as

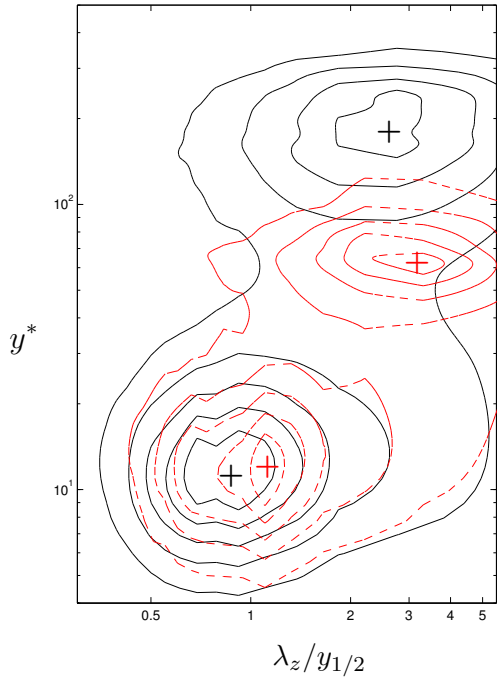

FIGURE 5.2. Premultiplied spanwise spectra, ${E^z_{uu}}^* = \lambda_z \Phi_{uu}/u_\tau^{*2}$, of the streamwise velocity fluctuations, isothermal case (black, solid) and exothermic case (red, dashed), scaled in the semi-inner scaling. The downstream position is $x/h = 25$ and figure is taken from Pouransari *et al.* (2013).

explained in eqs. (4.8) and (4.9), ${E^z_{uu}}^* = \lambda_z \Phi_{uu}/u_\tau^{*2}$. A corresponding wavelength in the semi-local scaling as $\lambda_z^* = \frac{2\pi}{\kappa_z} u_\tau^*/\nu$, could not be defined, since due to the density variation along the wall-normal axis, a different wavenumber for each wall-normal location and therefore different wavelengths would be needed. Thus, the local half-height of each jet has been used to demonstrate the corresponding wavelengths. The spectra have two peaks; the inner peak, which corresponds to the near-wall streaks and the outer-peak, which corresponds to the large energetic structures of the outer-layer. The figure confirms that the inner peak location is located approximately at the same distance from the wall for both isothermal and exothermic cases, but for the latter the peak is shifted to somewhat larger scales. The location of the outer peak is shifted significantly toward the inner region and to slightly larger scales, due to the heat release effects.

There are different possible approaches to describe the heat release effects on the small scales of turbulence. One way is to examine the higher

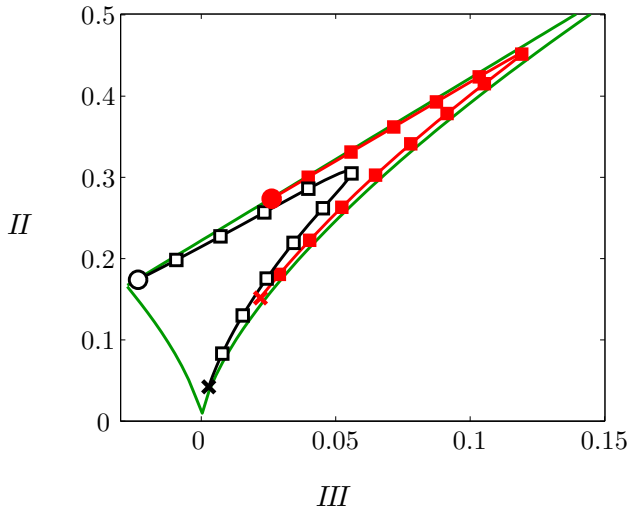

FIGURE 5.3. Anisotropy invariant maps for the SGS stress anisotropy at downstream position $x/h = 33$ for the isothermal and exothermic cases. Line styles are as follows; — ▫ — : isothermal case; — ▪ — : exothermic case. The circle marks indicate values at the wall and the cross signs show the corresponding values at $y^+ = 30$ for each case. Figure is taken from Pouransari *et al.* (2015*b*).

order moments of the gradient fields, that has a rather theoretical perspective, see Pouransari *et al.* (2015*a*). Another strategy, which has a more practical relevance, is to investigate the subgrid scale (SGS) statistics instead, see Pouransari *et al.* (2015*b*). Interestingly, the findings regarding the turbulence small-scale characteristics, gained through the statistical analysis of the flow have many phenomenological parallels with those concerning the SGS statistics. To characterize the heat-release effects on the SGS stress anisotropy tensor, invariant maps (Lumley & Newman 1977; Lumley 1978) are presented by cross-plotting the second II and third III invariants of the SGS stress anisotropy tensor $a_{ij} = \tau_{ij}/\tau_{kk} - \delta_{ij}/3$, defined as

$$II = a_{ij}a_{ij}, \quad III = a_{ik}a_{kj}a_{ji}\,. \tag{5.2}$$

The limits in the anisotropy invariant map correspond to the two-component turbulence state when $II = 2/9 + 2III$ and axisymmetric turbulence state when $II = 3/2(4/3|III|)^{2/3}$. These limits define a triangle in the anisotropy invariant map within which all the physically realizable turbulence states lie. In the anisotropy invariant map, isotropic turbulence with zero anisotropy corresponds to the lower corner of the triangle. Axisymmetric turbulence corresponds to the left and right edges of the triangle. At the left edge, one component of velocity fluctuations is smaller than the other two, while at the right

edge, one component of velocity fluctuations dominates the other two. The latter is denoted by axisymmetric expansion and the former by axisymmetric contraction. The upper edge of the triangle corresponds to the two-component turbulence as in turbulence near solid walls.

The anisotropy invariant maps are given in figure 5.3. The SGS anisotropy level increases due to the heat release effects in the entire wall-normal direction. At the wall, the trajectory of the isothermal case starts very close to the left branch, corresponding to the axisymmetric turbulence, whereas the starting point for the exothermic case, lies somewhere in the two-component limit (the upper edge). Close to the wall, around $y^+ = 7$, a maximum occurs in profiles of the two cases with a substantially higher value for the exothermic case than the isothermal one. This behavior is similar to what was observed in the total stress anisotropy map characteristics (Pouransari *et al.* 2015*a*), but is more accentuated for the SGS stress anisotropy. Further away, at $y^+ = 30$, the trajectories move towards the lower part of the right edge. While the isothermal trajectory gets very close to the lower corner of the triangle, the exothermic one lies somewhere on the right edge. This is consistent with the fact that the lower corner of the anisotropy invariant map represents an isotropic turbulence energy distribution, and indeed, the flow exhibits more isotropic characteristics for the isothermal case.

5.2. Heat release effects on the turbulent wall-jet flame

Illustrating the mixture fraction isosurface is perhaps the most classical way to visualize the flame in a non-premixed combustion regime. In addition, the maximum heat release is indeed concentrated in the vicinity of the stoichiometric condition. This is an important iso-plane in reacting flows, since this is the plane where the fuel and oxidizer should react optimally. Thus, the flame-turbulence interactions and heat release effects on the structure of the flame may be assessed by visualizing the stoichiometric mixture surface. The shape of this surface illustrates the wrinkling caused by turbulence, which can be substantially affected by the heat release effects, caused by the chemical reaction.

Figures 5.4(a) and (b) show the stoichiometric surfaces. Here, it can be observed that this surface develops in the downstream position into a highly wrinkled and deformed surface for the isothermal reacting case and the surface area per unit length in the $x-$direction increases considerably. This wrinkling is significantly damped in the exothermic case, due to the high heat release.

As was discussed in chapter 3, the scalar dissipation rate, $\chi = 2\overline{\rho\mathcal{D}\frac{\partial\theta''}{\partial x_i}\frac{\partial\theta''}{\partial x_i}}$, is a quantity of prominent importance in non-premixed combustion and therefore, it is important to understand the heat release effects on that. Often, some of the heat release effects are attributed to the decrease of the local Reynolds number, due to the chemical reaction (Pouransari *et al.* 2014). Here iso-contours of the scalar dissipation rate are illustrated in figure 5.5, for two

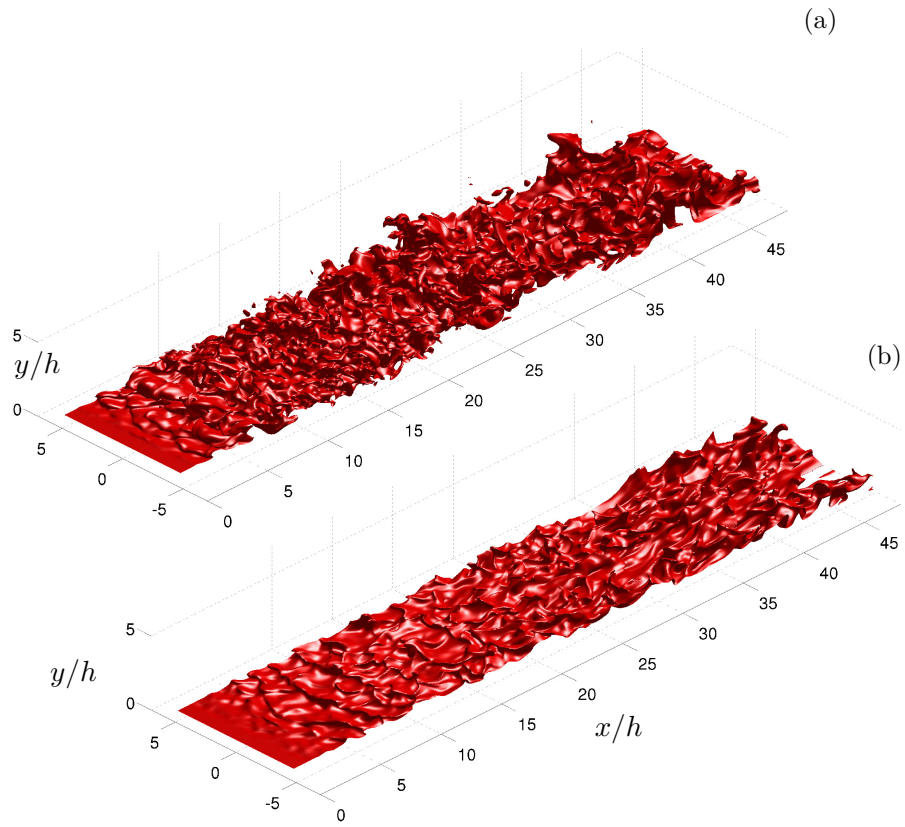

FIGURE 5.4. Stoichiometric mixture surface of (a) isothermal and (b) exothermic cases. Figure is taken from Pouransari *et al.* (2015*c*).

isothermal reacting cases with different Reynolds numbers. The fields are plotted on a logarithmic scale to accentuate their wide dynamic range. In both cases, long thin sheet-like structures are observed, similar to what is reported in Hawkes *et al.* (2007). These figures show much finer structures in the dissipation rate field of the higher Reynolds number case, indicating generation of more small scales due to the increase in the Reynolds number. In Pouransari *et al.* (2013), it was observed that the combustion heat release damp the small scales and merge them to larger structures. Here, with the increase in the Reynolds number, the trend is clearly the opposite and the structures become finer.

Another important point that can be deduced from figure 5.5 is that with the increase in the Reynolds number, the magnitude of the scalar dissipation

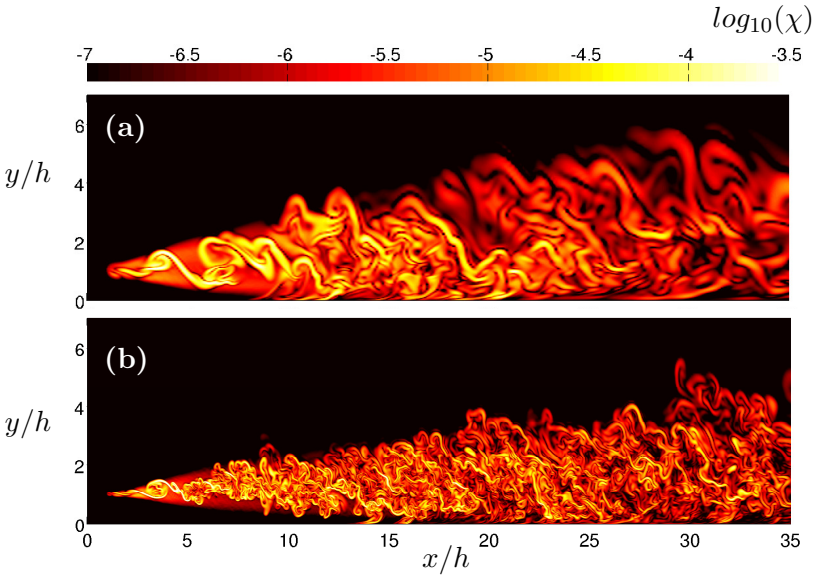

FIGURE 5.5. Iso-contours of the logarithm of the instantaneous scalar dissipation rate, (a) the lower ($Re = 2000$) and (b) higher ($Re = 6000$) Reynolds number cases. Figure is taken from Pouransari *et al.* (2014).

rate seems to be reduced. However, the scalar dissipation rate has the dimension of inverse time and is a representative of the small-scale mixing. Thus, when it decreases, the corresponding time scale increases.

Furthermore, the combustion heat release can also affect the characteristics of the reacting scalars. Using conditional statistics, in particular those conditioned on the mixture fraction, is a good way to visualize these effects.

The ramp-cliff contribution to the reactive scalar statistics in the reaction zone is much larger than the rest of the mixture fraction field. Thus, to better reflect the differences between the reactive scalars in the isothermal and exothermic cases, the conditional probability density functions (PDFs) on the mixture fraction are given in figure 5.6. Three different wall-normal positions, in terms of the local half-height of the jet, are chosen for the two cases. Note that the passive scalar concentration is used as the representative of the local mixture fraction. The PDFs of the reactive scalars are conditioned on the local mixture fraction. Around ten percent of the stoichiometric mixture fraction value $Z_{st} = 1/(1 + \phi r) = 0.33$, where $\phi = \theta_{F,inlet}/\theta_{O,inlet}$ is the equivalence ratio and $r = \nu_O/\nu_F = 1$ as is used in the reaction equation. It is observed that if a narrower range is chosen for the conditioning, the PDF tails become more damped and the corresponding peaks become sharper. It is notable that the PDFs of the reactive scalar derivatives, as observed in figure 5.6(b) are more skewed toward the negative side in the conditional plots than the corresponding

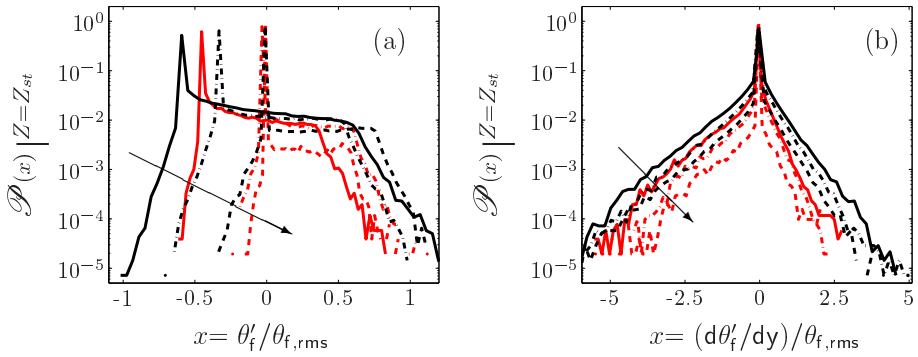

FIGURE 5.6. Probability density functions of (a) the reacting species and (b) the wall-normal gradient of the same scalars, conditioned on the mixture fraction at $x/h = 25$ at several wall-normal locations; black color is used for the isothermal case and the red color for the exothermic case; Line styles are as following: – – : $y/y_{1/2} = 0.5$ – · – : $y/y_{1/2} = 0.75$ and — : $y/y_{1/2} = 1.0$. Arrows point in the direction of decreasing $y/y_{1/2}$, i.e. moving closer to the wall. Figure is taken from Pouransari *et al.* (2015*a*).

unconditional PDFs. In particular, this is observed in the reaction zone and in the center of the flame at $y/y_{1/2} = 1.0$, which is similar to what is found in the anisotropic ramp-cliff like structures.

5.3. Heat release effects on the wall heat transfer

The heat transfer to the wall increases with increasing thermal energy release. The effective wall heat transfer in the chemically reacting wall-jets can be assessed by computing the corresponding Nusselt number as

$$Nu = \frac{\overline{Q_w}}{\lambda \Delta T\,/y_{1/2}}, \tag{5.3}$$

where $Q_w = -\lambda \left(\frac{dT}{dy}\right)_{wall}$ is the instantaneous wall heat flux, $y_{1/2}$ is the corresponding half-height of each jet and ΔT denotes a comparable temperature difference in the average temperature profile of each chemically reacting jet at the particular downstream position.

Since the half-height of the wall-jet is only weakly modified by the heat release effects (Pouransari *et al.* 2013), the conclusions about the Nu behavior remain the same, regardless of the choice of the outer length scale. However, the choice of ΔT makes a meaningful difference in the resulting Nusselt numbers for the different chemically reacting jets. We have chosen $\Delta T = T_m - T_w$, where T_w is the solid surface temperature, equal in all cases, and T_m is the maximum of the mean temperature profile. It can be observed in figure 5.7

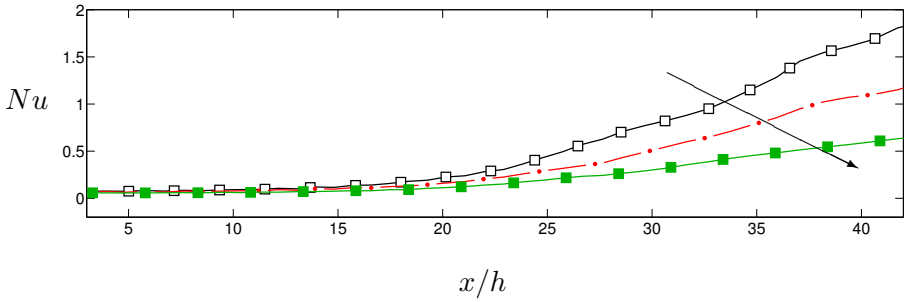

FIGURE 5.7. Downstream development of the mean wall heat flux scaled as Nusselt number. Line styles are as follows: —□— : exothermic case II, ($Ze = 8$, $Ce = 38$); —•— : exothermic case III, ($Ze = 7$, $Ce = 38$); —■— : exothermic case IV, ($Ze = 8$, $Ce = 40$). Arrow points in the direction of increasing heat release. Figure is taken from Pouransari *et al.* (2015*c*).

that the Nusselt number decreases with increasing heat release, i.e. $Nu_{II} > Nu_{III} > Nu_{IV}$. The trend is the same using other outer length scales for computing the Nusselt number. This is due to the fact that even though the absolute value of the heat flux is increasing, the maximum temperature in the mean profile is also increasing for cases III and IV, which results in a reduction of the Nusselt number. In other words, the effective heat transfer to the wall is reduced for cases with a higher heat release, due to reduced turbulent mixing. The turbulent kinetic energy also decreases with increasing heat release, see Pouransari *et al.* (2013).

For the same exothermic cases presented in figure 5.7 and a corresponding isothermal reacting case, the mean mass reaction rates are given in figures 5.8(a) and (b) at the downstream position $x/h = 33$. The reaction rate is normalized by the corresponding maximum inlet value of each simulation, $\dot{\omega}_{inlet} = Da\,\rho_j^2\,\Theta_{o,j}\,\Theta_{f,j}\;exp(-Ze/T_j)$. The reaction mainly takes place around the $y = y_{1/2}$ plane. This is also consistent with the snapshot of the reaction rate, shown in figure 4.2(b). Figure 5.8(a) shows that the maximum burning rate increases with the increase of the heat release, while in the near-wall region, an opposite trend is observed. To illustrate the near-wall behavior, the burning rate is given with the logarithmic scale in figure 5.8(b). The wall-cooling effect of the isothermal surface results in decrease of the local burning rate. Thus, the exothermic cases show a lower reaction rate for the near-wall region up to $y^+ = 30$, compared to the isothermal case. Figure 5.8(c) shows the burning rates scaled with their maximum values. The average profiles with this scaling retrieve a very similar shape, however, the near-wall characteristics of the burning rates, as observed in figure 5.8(d), still accentuate the wall cooling effect even when scaled with the maximum value.

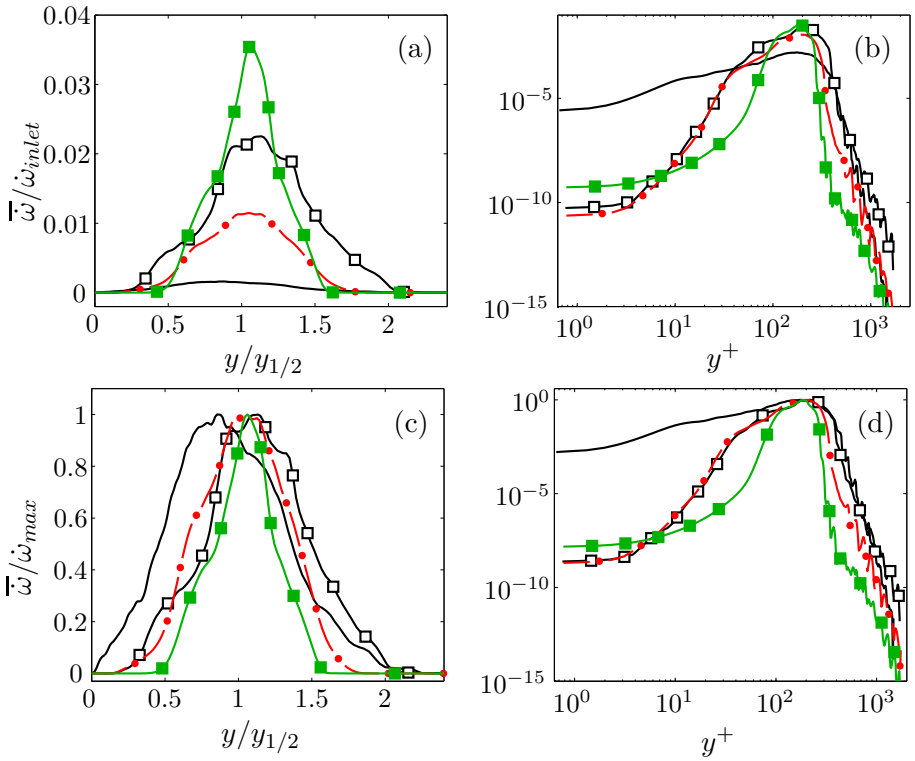

FIGURE 5.8. The mean mass reaction rate normalized in terms of inlet values in (a) linear and (b) logarithmic scale and normalized in terms of the maximum mean value in (c) linear and (d) logarithmic scale. Profiles are at the downstream position $x/h = 33$ and for the scaling of the linear plots the half-height of the jet $y_{1/2}$ is used for wall-normal direction and in the logarithmic plots y^+ is used. Line styles are as follows: ——— : isothermal case I; —□— : exothermic case II, ($Ze = 8$, $Ce = 38$); — • — : exothermic case III, ($Ze = 7$, $Ce = 38$); —■— : exothermic case IV, ($Ze = 8$, $Ce = 40$). Figure is taken from Pouransari *et al.* (2015*c*).

The flame structure depends on the different mixing and turbulence statistics, but it also depends on the prescribed parameters describing the reaction rate. Flames may possess different shapes, due to the difference in the reaction rate parameters. For instance, the Damköhler number that appears in the reaction rate formulation, can influence the reaction zone structure and the reactive scalars (Miller *et al.* 1994). Therefore, conclusions about the heat release effects cannot be drawn without considering its influence. To distinguish between the heat release and the Damköhler number effects, a comparison between two

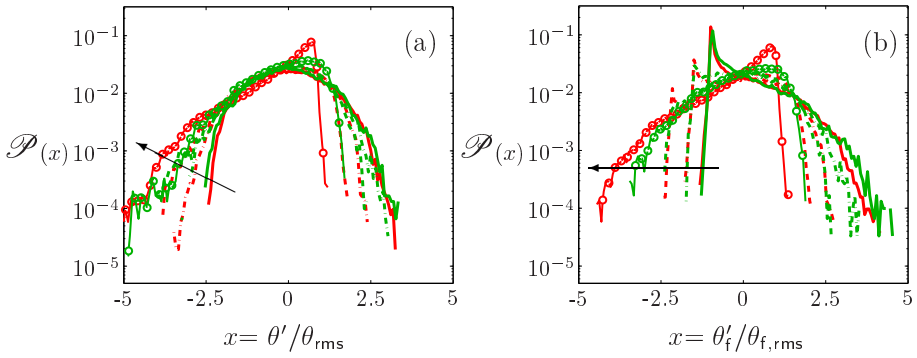

FIGURE 5.9. Probability density functions of (a) the passive scalar and (b) reactive scalars at $x/h = 25$ at several wall-normal distances; red color is used for the higher Damköhler number case ($Da = 1100$) and the green color for the lower Damköhler number case ($Da = 500$); Line styles are as following: —○— : $y/y_{1/2} = 0.25$, – – : $y/y_{1/2} = 0.5$, – · – : $y/y_{1/2} = 0.75$ and —— : $y/y_{1/2} = 1.0$. Arrows point in the direction of decreasing $y/y_{1/2}$. Figure is taken from Pouransari *et al.* (2015*a*).

exothermic DNS cases with different Damköhler numbers, of $Da = 500$ and 1100, is performed. Figure 5.9 shows the PDFs of both the passive and reactive scalars for these two cases. Four different wall-normal positions, in terms of the local half-height of the jet $y_{1/2}$, are considered. As expected, the turbulent flame becomes thinner with increasing Damköhler number, however, a similar dynamical behavior for the flame at the same wall-normal distance in terms of $y_{1/2}$ is expected. The two cases have similar characteristics at almost the entire wall-normal direction, except in the near-wall region at $y_{1/2} = 0.25$. This is where the Damköhler number effects are dominant and the PDF of the case with a higher Damköhler number is more skewed toward the negative side and obtains a higher peak value. This can also be associated with the isothermal wall cooling effects in the near-wall region.

CHAPTER 6

Summary of the papers

Paper 1

Direct numerical simulation of an isothermal reacting turbulent wall-jet

We have performed direct numerical simulation (DNS) of a reacting turbulent wall-jet. A single-step global reaction is considered in which the reaction rate is temperature independent. In this study, thermal effects of the chemical reaction are neglected intentionally, to exclusively concentrate on the turbulent flow effects on the isothermal reaction. Fuel and oxidizer enter the computational domain in two separate streams. The jet flow consist of fuel and the coflow contains the oxidizer species.

The turbulent statistics of the present DNS are validated against previous DNS of a non-reacting turbulent wall-jet. To shed light on turbulent mixing effects on concentration fields in the near-wall region, a detailed study of the probability density functions (PDFs) is carried out. The comparison between the reacting and passive scalar PDFs throughout the domain, reveals the significance of the reaction influence and the wall effects on the scalar distributions. A detailed discussion about the scalar dissipation rate of the conserved and reacting scalars is included. Further, the higher order moments of the scalar concentrations as well as the velocities are examined. The higher order moments of velocities exhibit a similar behavior to those of other wall-bounded flows. Moreover, the fundamental features of the reaction rate are illustrated through the instantaneous fields and stoichiometric mixture surface in the isothermal reacting turbulent wall-jet. Furthermore, a comparison between the third order moments of velocities with the recent experimental measurements is made, which shows an acceptable correspondence.

Paper 2

Heat release effects on mixing scales of turbulent reacting wall-jets, a direct numerical simulation study

This study concerns the role of heat release in chemically reacting turbulent wall-jet flows, where DNSs of several chemically reacting turbulent wall-jets including significant amounts of heat release are performed. The main aim

of this investigation is to examine the heat-release effects on different scales of turbulence. The "turbulence-chemistry" or more precisely "turbulence-heat release" interactions are illustrated by studying the modifications of different large and mixing scales. The influence of heat release on different turbulence and reactants statistics is investigated.

Primarily, it is observed that heat release effects delay the transition process in the chemically reacting cases and enlarge the fluctuation intensities of density and pressure. Heat release also enhances the fluctuations level of the species concentrations. However, it has a damping effect on all velocity fluctuation intensities as well as the Reynolds shear stress. The turbulent kinetic energy behavior in different cases is examined, using different scalings. Mixing scales are visualized by exploring the dissipation rate of the fuel and passive scalar concentrations. We observed much finer structures in the isothermal reacting turbulent wall-jet and found that heat release modifies both the instantaneous field characteristics and the mean values of the scalar dissipation rates. With aid of vortex diagnosing tools, the stoichiometric mixture fraction surface and the two-point correlations of velocities, heat-release consequences on different scales are identified. Larger vortices are detected in simulations with a higher amount of heat-release and some of the smaller structures are merged together.

Further analysis using one-dimensional and two-dimensional premultiplied spectra of the streamwise velocity are performed, where the results indicate a shifting in the position of the outer peak of the energy spectra. Moreover, probability density functions of reactants are found to be affected by heat release effects. Finally, the scatter plots of the burning rate versus the inverse of the scalar dissipation rate and also temperature fields against the mixture fraction are studied at different locations.

Paper 3

Statistical analysis of the velocity and scalar fields in reacting turbulent wall-jets

In this paper, the DNS database of the isothermal and exothermic reacting turbulent wall-jets, obtained in our previous studies are used, in order to extract information about the heat release effects on the small-scales of turbulence. The problem of quantifying anisotropic and non-Gaussian fluctuations is addressed in chemically reacting turbulent wall-jet flows, with different combustion properties (isothermal and exothermic) and varying the measuring location, for several wall distances.

Fully passive components, passive but reactive and active scalars are examined. In particular, probability density functions of different scalars are studied to understand the heat release and chemical reaction effects on both the large and small scale characteristics of the flow. The chemical reaction and heat-release effects are found to be significant in different regions of the flow. In the near wall-region, the heat release effects dominate, while in the outer region of

the jet, the chemical reaction influences are overwhelming. By analyzing the statistics of the scalar fields, the importance of combustion is illustrated, in regions far from the wall, where a high intermittency is measured due to the depletion of the fuel. Two exothermic cases with different Damköhler numbers are examined and the comparison revealed that the Damköhler number effects are most dominant in the near-wall region, where the wall cooling effects are influential. In addition, with the aid of PDFs conditioned on the mixture fraction, the significance of the reactive scalar characteristics in the reaction zone is illustrated.

Moreover, the anisotropy invariant maps for the Reynolds stress tensor are investigated to illustrate the heat release effects on the anisotropy level of the large scales. The higher order moments of the velocity and scalar fields at large and small scales, are employed to further characterize the anisotropies at both large and small scales. For instance, the skewness of a vector field, defined in terms of any of its components, is zero in an isotropic field, but the situation is different if the gradients are considered where only the odd moments of the transverse gradients must vanish in an isotropic ensemble, while the longitudinal ones can be (and indeed are) different from zero also in a purely rotational invariant case. Therefore, if the wall-normal derivatives are considered, the skewness of the streamwise and spanwise components are expected to be genuine measurements of the degree of anisotropy, while the skewness of the wall-normal component itself is not, being affected by both isotropic and anisotropic fluctuations.

Looking at the statistics of the gradients, the presence of a strong persistency of anisotropy at small-scales affecting both the velocity and scalars are highlighted, even at large distances from the wall. Intermittent non-Gaussian fluctuations are found to be strong also for isotropic components. We argue that the departure from isotropic characteristics in the entire domain can affect mixing and ultimately the combustion characteristics of the reacting flow. The combined effects of strong intermittent corrections and strong persistency of anisotropy at small scales have implications for the development of more accurate subgrid-scale (SGS) models.

Paper 4

DNS analysis of wall heat transfer and combustion regimes in a turbulent non-premixed wall-jet flame

Understanding the heat-release effects on the wall heat transfer in turbulent reacting flows, i.e. heat transfer with or without significant density variation, is essential for a wide variety of industrial flows, especially combustion problems. The present study focuses on the wall heat transfer and the near-wall reaction characteristics.

New direct numerical simulations (DNSs) of turbulent reacting flow with heat-release are performed in the wall-jet configuration in a larger computational domain than the preceding studies in paper 2. In particular, a longer streamwise length is chosen, hence, there is more room for studying the wall-turbulence and flame-wall interactions. Significant variations in the density and temperature fields are observed and the compressibility and heat-release effects on the density and temperature fluctuation intensities are addressed.

The heat-release effects on the skin-friction coefficients, C_f are investigated comparing DNSs of isothermal and exothermic reacting turbulent wall-jets. Reductions in the C_f are observed in the exothermic case, compared to the isothermal one, and it is found that, the underlying mechanisms responsible for the behavior of the C_f are different at different regions of the domain and are explained accordingly.

The wall heat transfer rates are examined for the different reacting cases. The absolute wall heat flux is increased due to the substantial temperature rise in the flow field, however, the effective wall heat transfer, measured with the corresponding Nusselt number, decreases with increasing heat release. Furthermore, the cold wall effects on the near-wall average burning rate are assessed. It is found that the isothermal wall cooling effect results in an appreciable decrease of the burning rate in the exothermic cases.

The flame structure is further analyzed using the flame index and the scatter plots for the relative angle between the gradients of the fuel and oxidizer scalar fields. Finally, the scatter plots are also used to illustrate the coupling between the local concentration of the reactants and mixture fraction. The scatter plots indicate that the presence of the wall increases the chances for the development of the premixed mode.

Paper 5

Assessment of subgrid-scale stress statistics in non-premixed turbulent wall-jet flames

Heat release effects on the small scales of turbulence can be described with different approaches. From a theoretical perspective, the higher order moments of the gradient fields, representing the small-scale characteristics, were studied in paper 3. In the present investigation, a more practical technique is used. An analysis of the subgrid-scale (SGS) statistics has been carried out, to study the heat-release effects, using direct numerical simulation (DNS) data of a turbulent reacting wall-jet flow. Some phenomenological analogy between the small-scale characteristics, gained through the statistical analysis of the flow, with those concerning the SGS statistics, were expected to be found.

Two sets of DNS data are employed, one includes an isothermal reaction and the other is an exothermic one with heat release. In particular, the properties of the SGS stress tensor, SGS dissipation of kinetic energy and enstrophy

are investigated. The separation of scales, to obtain the SGS quantities, is achieved by application of a box filter.

In addition, the heat release has a considerable influence on the relative alignment of the SGS stress and resolved strain tensors. Analysis of the PDFs of the cosine of the angle between the eigenvectors, corresponding to the largest eigenvalue of the two tensors, shows that the alignment is increased in the buffer layer, while it is decreased away from the wall. The important degree and variation of the non-alignment between the SGS stress and resolved strain-rate tensors represents an important indication of the need for SGS stress models that are more advanced than the eddy-viscosity-based ones.

To find out the heat-release effects on the dynamics of the turbulent energy dissipation, SGS dissipation of kinetic energy and enstrophy are evaluated using length-scale, probability density functions (PDFs) and mean value analysis. It is found that the mean SGS shear stress and turbulent kinetic energy are suppressed by the heat release, while the SGS anisotropy is substantially increased. Although, the topology of the resolved strain-rate tensor only marginally differs between the isothermal and exothermic cases in the near-wall wall region, substantial differences are observed in the shear layer in the jet area, where the compressibility effects are important and the exothermic effects are found to promote compression states. Analysis of the eigenvectors of the resolved strain-rate tensor shows that extension is the dominant state, in the isothermal case, while in the exothermic case, compression state is more dominant in the jet area of the flow. A similar test of the SGS stress tensor reveals that, contrary to the resolved strain-rate tensor, compression state is dominant for this tensor and the heat release promotes it.

The SGS stress anisotropy is observed to increase everywhere in the flow with the increase of the heat release. The mean SGS dissipation was found to increase in the near-wall region and decrease in the jet area. The PDFs show an increased intermittency in the SGS dissipation in the buffer layer in the exothermic case, while the opposite occurs further away from the wall. Further analysis of the SGS dissipation shows that its length scale is substantially affected, especially in the jet area where the heat-release effects are observed, leading to much larger length scales in the exothermic case. Finally, the SGS dissipation of enstrophy is studied, where the heat-release effects are found to decrease the mean SGS enstrophy dissipation and its intermittency in the near-wall region.

Paper 6

Reynolds number effects on statistics and structure of an isothermal reacting turbulent wall-jet

In this study, the Reynolds number effects on statistics and structure of isothermal reacting turbulent wall-jets are addressed. So far, in our previous studies,

the Reynolds number was kept constant in order to focus on other points of interest, especially the heat release effects. The heat release effects, however, are frequently attributed to the decrease of the local Reynolds number, due to the chemical reaction, which needs to be further explored using a range of Reynolds numbers.

Thus, in this study, a three-dimensional direct numerical simulation (DNS) of an isothermal reacting turbulent wall-jet is performed at a substantially higher Reynolds number than our previous studies. In this study, the bulk Reynolds number of the flow, in terms of the inlet quantities, varies from $Re = 2000$ to $Re = 6000$, which results in a comparable change in friction Reynolds numbers. The flow configurations, boundary conditions and the structure of the flame are all similar to the isothermal non-premixed wall-jet flame, presented in paper 1. In the higher Reynolds number simulation case, the grid resolution employs about 180million cells and is well resolved.

Both the turbulent and flame structures become much finer at the higher Reynolds number. The effect of decreasing the Reynolds number and adding the combustion heat release are compared with each other and found to be similar for some aspects of the flow. Key quantities such as the scalar dissipation rate, reaction rates and the turbulent kinetic energy profiles are discussed thoroughly. The discussion is complemented by illustrating the Reynolds number effects on the premultiplied spectra. Considering both the Taylor micro scale and the Kolmogorov scale as well as the half-height of the wall-jet, the effects of increasing the Reynolds number on a wide range of length scales are recognized. In light of the knowledge gained from the changes in different length and time scales, a detailed description of how the reaction would differ for the higher Reynolds number case compared to the lower Reynolds number case is provided.

CHAPTER 7

Concluding remarks and outlook

This study was focused on understanding the triple "flame-turbulence-wall" interactions in reacting turbulent wall-jet flames, using direct numerical simulation (DNS). The heat release effects on the large and small scales of turbulence were extensively investigated for mixing and combustion applications. Larger vortices and flame structures were detected and some of the smaller structures are merged together in simulations with a higher amount of heat-release. Statistics of the gradients reveal the presence of a strong persistency of anisotropy at small-scales, for both the velocity and scalars. The combined effects of the strong intermittency and persistency of anisotropy at small scales have implications for the development of subgrid-scale (SGS) models. An analysis of the SGS statistics has been carried out, to study the heat-release effects, using the obtained DNS databases. Some parallels between the small-scale characteristics, gained through the statistical analysis of the flow, with those concerning the SGS statistics, are found. Moreover, the wall-jet configuration enabled us to study different wall effects on the turbulence and flame structure. The heat-release effects on the wall heat transfer are investigated. It is found that the wall cooling effect results in an appreciable decrease of the burning rate in the exothermic cases and the presence of the wall increases the chances for the development of the premixed mode. However, more detailed information about the flame-wall interaction may be gained by introducing a multi-step reaction with sufficient chemistry.

A DNS of an isothermal reacting turbulent wall-jet was also performed at a substantially higher Reynolds number than our previous studies, to seek information about the differences of the mixing scenario in the near-wall region and the impact on the flame structure. In light of the knowledge gained from the Reynolds number effects on the different flow scales, a detailed description of the differences in the reaction characteristics is provided. The higher Reynolds number DNS database can be used to further analyze the SGS statistics in compressible flows, such as the SGS scalar flux and scalar variance characteristics to evaluate non-premixed combustion models.

Furthermore, examination of exothermic DNSs with different Damköhler numbers revealed that the Damköhler number effects are most dominant in the near-wall region. An appropriate next step is to perform DNSs at a wider range of flow and reaction parameters.

Acknowledgments

I would like to acknowledge my supervisor Prof. Arne V. Johansson for his supportive accompaniment, enthusiastic leadership and encouraging inspirations and his guidance and generosity during my work in the past few years. Thanks Arne, for sharing your knowledge in turbulence with me and for trusting me as an independent researcher. Your always positive attitude towards my ideas and works are greatly appreciated.

Next, I would like to thank Prof. Luc Vervisch, for being the "combustion" advisor for me, throughout most of this work. Your quick and constructive responses to my work and your outstanding teaching attitude are very much appreciated. Your positive and favorable standpoint was always a great source of encouragement for me.

I would like to thank the coauthors of the papers in this thesis. Arne Johansson, Luc Vervisch, Luca Biferale, Laszlo Fuchs, Geert Brethouwer and Amin Rasam. I gratefully acknowledge Prof. Luca Biferale for the fruitful discussions we had, during his visits to KTH, while we met in conferences elsewhere and also during several online meetings. Thanks for your time and patience and your strong will to convey your insight about turbulence to me. Prof. Laszlo Fuchs is specially thanked, for his comments on my work and for being the source of combustion assurance for me inside the department.

I would also like to acknowledge my co-advisors, Dr. Geert Brethouwer and Dr. Stefan Wallin for their helps and discussions.

This thesis has been proofread by Dr. Amin Rasam, Dr. Ramis Örlü and Dr. Stefan Wallin, their feedbacks and useful comments are very much appreciated.

Prof. B. J. Boersma, is acknowledged for providing the original version of the simulation code and Dr. Daniel Ahlman is thanked for his initial helps with the code.

This project has been financed by the Swedish Centre for Combustion Science and Technology (CECOST), which I would like to gratefully acknowledge and also specially thank all the members of "modeling and validation group". I have been overwhelmed with many other scholarships and awards, twice the Erik Petersohns Minne fund and also the Odqvist award of the Swedish mechanics days, thanks.

I would like also to thank the Swedish National Infrastructure for Computing (SNIC) for providing the computer time and convey my deepest gratitude to the support team at PDC.

During a three-month visit I had to CORIA laboratory in Rouen, France, I enjoyed a warm hospitality by the group there, I would like to specially thank, Luc, Pascal, Yves, Guillaume, Vincent, Catherine, Ghislain, Marianne, Cindy and many others for their supportive reception.

I would like to thank all my past and present officemates for the pleasant working atmosphere in our room and many thanks to colleagues at the Mechanics department of KTH; You made it a pleasure for me to come to work everyday, I would like to specially name, Dr. Ardeshir Hanifi, Olof, Werner, Igor, Xuina, Priti, Yang, Ruoli, Mireia, Lanie, Armin, Natalia, Zeinab, Timea, Nima, Carolina, Iman, Lisa, Outi, Shervin, Mihai, Anders D., Arne N., Hanno, Jiewei, Reza, Taras, Nicolo, Mattias, Jacopo, Ricardo, Johan, Enrico, Robert, Onofrio, Antonios, David, Qiang, Lailai, Lars-Uve, Daniel, Erik, Ugis, Eva, Shahab, Alessandro, Antonio, Ramis, Bengt, Sohrab, Tobias, Ylva, Sissy, Alexandra, Julie, Azad, Sasan, Andreas, Amer, Elinor, Ramin and many others from the Lab and at OB18. Very special thanks to our kind and supportive administrative personnel, Carolina, Heide, Malin and Pär.

Finally, I wish to give my heartfelt thanks to my parents, my grandmother, my brother and sisters, my kind family in law and other family members for their constant care, continuous encouragements and unconditional supports. I feel so blessed and proud of such a nice family.

To my loved ones, my dear Amin and our lovely and adorable son Zackaria. Zackaria, you have filled our life with so much joy and happiness. During the last months, you took me to and from university every morning and afternoon and waved byebye to me, which melted my heart and made me feel so special, this was really memorable for me!
Amin, my husband and my best friend of more than a decade, your scientific contributions to this thesis are countless and invaluable. Thank you so much for your helps, support, endless love, understanding and patience, which made all this possible.

Bibliography

Ahlman, D. 2007 Numerical studies of turbulent wall-jets for mixing and combustion applications. PhD thesis, Royal Institute of Technology, KTH, Stockholm, Sweden.

Ahlman, D., Brethouwer, G. & Johansson, A. V. 2007 Direct numerical simulation of a plane turbulent wall-jet including scalar mixing. *Phys. Fluids* **19**, 065102.

Ahlman, D., Velter, G., Brethouwer, G. & Johansson, A. V. 2009 Direct numerical simulation of non-isothermal turbulent wall-jets. *Phys. Fluids* **21**, 035101.

Baritaud, T., Poinsot, T. & Baum, M. 1996 *Direct Numerical Simulation for Turbulent Reacting Flows*. Editions Technip.

Bilger, R. W. 2000 Future progress in turbulent combustion research. *Prog. Energy Combust. Sci.* **26**, 367–380.

Boersma, B. J. 2004 Numerical simulation of the noise generated by a low Mach number, low Reynolds number jet. *Fluid Dyn. Res.* **35**, 425–447.

Bradshaw, P. & Gee, M. T. 1960 Turbulent wall-jets with and without external stream. *Aeronautics Research Council Reports and Memoranda* **No. 3252**.

Bruneaux, G., Akselvoll, K., Poinsot, T. & Ferziger, J. H. 1996 Flame-wall interaction simulation in a turbulent channel flow. *Combust. Flame* **107**, 27–44.

Bruneaux, G., Poinsot, T. & Ferziger, J. H. 1997 Premixed flame-wall interaction in a turbulent channel flow: budget for the flame surface density evolution equation and modeling. *J. Fluid Mech.* **349**, 191–219.

de Bruyn-Kops, S. M., Riley, J. J., Kosaly, G. & Cook, A. W. 1998 Investigation of modeling for non-premixed turbulent combustion. *Flow, Turbul. Combust.* **60**, 105–122.

Cant, R. S. & Mastorakos, E. 2007 *An Introduction to Turbulent Reacting Flows*. Imperial College Press.

Chen, J. H. 2011 Petascale direct numerical simulation of turbulent combustion–fundamental insights towards predictive models. *Proc. Combus. Inst.* **33**, 99–123.

Conaire, M. O., Curran, H. J., Simmie, J. M., Pitz, W. J. & Westbrook, C. K. 2004 A comprehensive modeling study of hydrogen oxidation. *Int. J. Chem. Kinet.* **36**, 603–622.

Conlon, B. P. & Lichter, S. 1995 Dipole formation in the transient planar wall-jet. *Phys. Fluids* **7**, 99–114.

Cook, A. W., Riley, J. J. & Kosaly, G. 1997 A laminar flamelet approach to subgrid-scale chemistry in turbulent flows. *Combust. Flame* **109**, 332–341.

Dabrieau, F., Cuenot, B., Vermorel, O. & Poinsot, T. 2003 Interaction of flames of $H_2 + O_2$ with inert walls. *Combust. Flame* **135**, 123–133.

Damköhler, G. 1947 The effect of turbulence on the flame velocity in gas mixtures. *NACA, Tech. Memo. No. 1112* **46**, 601.

Davidson, P. A. 2004 *Turbulence: An introduction for scientists and engineers*. OXFORD.

Dejoan, A. & Leschziner, M. A. 2005 Large Eddy Simulation of a plane turbulent wall jet. *Phys. Fluids* **17**, 025102.

del Álamo, J. C. & Jiménez, J. 2003 Spectra of the very large anisotropic scales in turbulent channels. *Phys. Fluids* **15** (6), 41–44.

Dey, S., Nath, T. K. & Bose, S. K. 2010 Submerged wall-jets subjected to injection and suction from the wall. *J. Fluid Mech.* **653**, 57–97.

Diez, F. J. & Dahm, W. J. A. 2007 Effects of heat release on turbulent shear flows. part 3. buoyancy effects due to heat release in jets and plumes. *J. Fluid Mech.* **575**, 221–255.

Dopazo, C. 1994 Recent developments in PDF methods. *Turbulent Reacting Flows, Academic Press London,* pp. 375–476.

Eriksson, J. G., Karlsson, R. I. & Persson, J. 1998 An experimental study of a two-dimensional plane turbulent wall jet. *Exp. Fluids* **25**, 50–60.

Falkovich, G., Gawedski, K. & Vergassola, M. 2001 Particles and fields in fluid turbulence. *Rev. Mod. Phys.* **73**, 913.

Förthmann, E. 1934 Über turbulente Strahlausbreitung. *Ing. Arch.* **5**, 42–54.

Fox, R. O. 2003 *Computational Models for Turbulent Reacting Flows*. Cambridge University Press.

Frisch, U. 1995 *Turbulence: The legacy of A.N. Kolmogorov*. Cambridge University Press.

Fureby, C. 2008 Towards the use of large eddy simulation in engineering. *Prog. Aerosp. Sci.* **44**, 381–396.

George, W. K., Abrahamsson, H., Eriksson, J., Karlsson, R. I., Löfdahl, L. & Wosnik, M. 2000 A similarity theory for the turbulent plane wall jet without external stream. *J. Fluid Mech.* **425**, 367–411.

Glassman, I. & Yetter, R. A. 2008 *Combustion*. Academic Press.

Glauert, M. B. 1956 The wall jet. *J. Fluid Mech.* **1**, 625–643.

Gogineni, S., Visbal, M. & Shih, C. 1999 Phase-resolved PIV measurements in a transitional plane wall jet: a numerical comparison. *Exp. Fluids* **27**, 126.

Gruber, A., Sankaran, R., Hawkes, E. R. & Chen, J. H. 2010 Turbulent flame-wall interaction: a direct numerical simulation study. *J. Fluid Mech.* **658**, 5–32.

Hall, J. W. & Ewing, D. 2010 Spectral linear stochastic estimation of the turbulent velocity in a square three-dimensional wall jet. *J. Fluids Eng.* **132** (051203).

Hawkes, E. R., Sankaran, R., Sutherland, C. & Chen, J. H. 2007 Scalar mixing in direct numerical simulations of temporally evolving plane jet flames with skeletal CO/H2 kinetics. *Proc. Combust. Inst.* **31**, 1633–1640.

Hilbert, R., Tap, F., El-Rabii, H. & Thévnin, D. 2004 Impact of detailed chemistry and transport models on turbulent combustion. *Prog. Energy Combust. Sci.* **30**, 61–117.

Hogg, A. J., Huppert, H. E. & Dade, W. B. 1997 Erosion by planar turbulent wall jets. *J. Fluid Mech.* **338**, 317–340.

Huang, P. G., Coleman, G. N. & Bradshaw, P. 1995 Compressible turbulent channel flows: DNS results and modelling. *J. Fluid Mech.* **305**, 185–218.

Hunt, J. C., Wray, A. A. & Moin, P. 1988 Eddies, stream and convergence zones in turbulent flows. *Tech. Rep. CTR-S88, Center for turbulence research, Stanford University* .

Knaus, R. & Pantano, C. 2009 On the effect of heat release in turbulence spectra of non-premixed reacting shear layers. *J. Fluid Mech.* **626**, 67–109.

Kolmogorov, A. N. 1941 The local structure of turbulence in incompressible viscous fluid for very large reynolds numbers. *In Dokl. Akad. Nauk SSSR* **30**, 299–303.

Krisman, A., Tang, J. C. K., Hawkes, E. R., Lignell, D. O. & Chen, J. H. 2014 A DNS evaluation of mixing models for transported PDF modelling of turbulent non-premixed flames. *Combust. & Flame* **161**, 2085–2106.

Launder, B. E. & Rodi, W. 1981 The turbulent wall jet. *Prog. Aerospace. Sci* **19**, 81–128.

Leonard, A. 1974 Energy cascade in large eddy simulations of turbulent fluid flows. In *Turbulent Diffusion in Environmental Pollution*, , vol. 1, pp. 237–248.

Levin, O., Chernoray, V. G., Löfdahl, L. & Henningson, D. S. 2005 A study of the Blasius wall jet. *J. Fluid Mech.* **539**, 313–347.

Livescu, D., Jaberi, F. A. & Madnia, C. K. 2002 The effects of heat release on energy exchange in reacting turbulent shear flow. *J. Fluid Mech.* **450**, 35–66.

Lumley, J. L. 1978 Computational modeling of turbulent flows. *Adv. in appl. Mech.* **18** (123), 213.

Lumley, J. L. 2007 *Stochastic tools in turbulence*. Dover.

Lumley, J. L. & Newman, G. R. 1977 The return to isotropy of homogeneous turbulence. *J. Fluid Mech.* **82**, 161–178.

McMurtry, P. A., Riley, J. J. & Metcalfe, R. W. 1989 Effects of heat release on the large-scale structure in turbulent mixing layers. *J. Fluid Mech.* **199**, 297–332.

Miller, M. S., Madina, C. K. & Givi, P. 1994 Structure of a turbulent reacting mixing layer. *Comb. Sci. Tech.* **99**, 1–33.

Mizobuchi, Y., Shinjo, J., Ogawa, S. & Takeno, T. 2005 A numerical study on the formation of diffusion flame islands in a turbulent hydrogen jet lifted flame. *Proc. Combust. Inst.* **30**, 611–619.

Monin, A. S. & Yaglom, A. M. 1975 Statistical fluid mechanics, volume II: Mechanics of turbulence. *Dover publication* .

Narashima, R., Narayan, K. Y. & Parthasarathy, S. P. 1973 Parametric analysis of turbulent wall jets in still air. *Aeronaut. J.* **77**, 335.

Neuendorf, R. & Wygnanski, I. 1999 On a turbulent wall jet flowing over a circular cylinder. *J. Fluid Mech.* **381**, 1–25.

O'Brien, E. E. 1980 The probability density function (PDF) approach to reacting turbulent flows. *Turbulent Reacting Flows, Academic Press London* p. 185.

Perot, B. & Moin, P. 1995 Shear-free turbulent boundary layers. Part 1. Physical insights into near-wall turbulence. *J. Fluid Mech.* **295**, 199–227.

Peters, N. 2000 Turbulent combustion. Cambridge University Press.

Pitsch, H. 2006 Large-eddy simulation of turbulent combustion. *Annu. Rev. Fluid Mech.* pp. 453–482.

Pitsch, H. 2010 Shedding new light on a burning question. *J. Fluid Mech.* **658**, 1–4.

Pitsch, H. & Trisjono, P. 2014 Can combustion models be developed from DNS data? In *19th Australasian Fluid Mechanics Conference, Melbourne, Australia*.

Poinsot, T., Candel, S. & Trouvé, A. 1996 Applications of direct numerical simulation to premixed turbulent flames. *Prog. Energy Combust. Sci.* **21**, 531–576.

Poinsot, T., Haworth, D. C. & Bruneaux, G. 1993 Direct simulation and modeling of flame-wall interaction for premixed turbulent combustion. *Combust. Flame* **95**, 118–132.

Poinsot, T. & Veynante, D. 2005 *Theoretical and Numerical Combustion*. R.T. Edwards.

Pope, S. B. 1985 PDF method for turbulent reacting flows. *Prog. Energy Combust. Sci.* **11**, 119–195.

Pope, S. B. 2000 *Turbulent flows*. Cambridge University Press.

Popov, P. P. & Pope, S. B. 2014 Large eddy simulation/probability density function simulations of bluff body stabilized flames. *Combust. & Flame* **161**, 3100–3133.

Pouransari, Z., Biferale, L. & Johansson, A. V. 2015*a* Statistical analysis of the velocity and scalar fields in reacting turbulent wall-jets. *Phys. Fluids* **27 (025102)**.

Pouransari, Z., Brethouwer, G. & Johansson, A. V. 2011 Direct numerical simulation of an isothermal reacting turbulent wall-jet. *Phys. Fluids* **23 (085104)**.

Pouransari, Z., Rasam, A., Vervisch, L. & Johansson, A. V. 2015*b* Assessment of subgrid-scale stress statistics in non-premixed turbulent wall-jets. *Submitted* .

Pouransari, Z., Vervisch, L., Fuchs, L. & Johansson, A. V. 2015*c* DNS analysis of wall-heat transfer and combustion regimes in a turbulent non-premixed wall-jet flame. *Submitted* .

Pouransari, Z., Vervisch, L. & Johansson, A. 2013 Heat release effects on mixing scales of non-premixed turbulent wall-jets: a DNS study. *Int. J. Heat and Fluid Flows* **40**, 65–80.

Pouransari, Z., Vervisch, L. & Johansson, A. V. 2012 Analysis of combustion modeling tools using DNS of a non-premixed turbulent wall-jet. *Seventh Intern. Symp. on Turbulence Heat & Mass Transfer, Sicily Italy* **7**, 705–708.

Pouransari, Z., Vervisch, L. & Johansson, A. V. 2014 Reynolds number effects on statistics and structure of an isothermal reacting turbulent wall-jet. *Flow, Turb. Combust.* **92**, 931–945.

Prandtl, L. 1932 Zur turbulenten Strömung in Rohren und längs Platten. *Ergebn. Aerodyn. Versuchsanst. Göttingen* **4**, 18–29.

Richardson, L. F. 1922 Weather prediction by numerical process. .

Riley, J. J. 1998 Turbulent combustion modelling. In *Transition, Turbulence and Combustion Modelling, Ercoftac Series* (ed. A. Hanifi, H. Alfredsson, A. V. Johansson & D. Henningson). Kluwer academic publishers.

Ruetsch, G. R., Vervisch, L. & Linan, A. 1995 Effects of heat release on triple flames. *Phys. Fluids* **7**, 1447–1454.

Sagaut, P. 2000 *Large eddy simulation for incompressible flows*, , vol. 3. Springer Berlin.

Seidel, J. & Fasel, H. F. 2001 Numerical investigations of heat transfer mechanisms in the forced laminar wall-jet. *J. Fluid Mech.* **442**, 191–215.

Shraiman, B. I. & Siggia, E. D. 2000 Scalar turbulence. *Nature* **405**, 639–646.

Tennekes, H. & Lumley, J. L. 1972 *A first course in turbulence*. The MIT Press.

Turns, S. R. 1993 *An introduction to combustion: Concepts and Applications*. McGraw Hill.

Vervisch, L. 2000 Using numerics to help the understanding of non-premixed turbulent flames. *Proc. Combust. Inst.* **28**, 11–24.

Vervisch, L., Bidaux, E., Bray, K. N. C. & Kollmann, W. 1995 Surface density function in premixed turbulent combustion modeling, similarities between probability density function and flame surface approaches. *Phys. Fluids* **10**, 2498–2503.

Vervisch, L. & Poinsot, T. 1998 Direct numerical simulation of non-premixed turbulent flames. *Annu. Rev. Fluid Mech.* **30**, 655–691.

Vervisch, L. & Veynante, D. 2011 Turbulent Combustion. Von Karman Institute for Fluid Dynamics.

Veynante, D. & Vervisch, L. 2002 Turbulent combustion modeling. *Prog. Energy Combust. Sci.* **28**, 1–138.

Visbal, M., Gaitonde, D. V. & Gogineni, P. 1998 Direct numerical simulation of forced transitional plane wall jet. *AIAA paper, 98-2643* .

Wall, C., Boersma, B. J. & Moin, P. 2000 An evaluation of the assumed beta probability density function subgrid-scale model for large eddy simulation of nonpremixed turbulent combustion with heat release. *Phys. Fluids* **12**, 2522–2529.

Wang, Y. & Trouvé, A. 2006 Direct numerical simulation of nonpremixed flame-wall interactions. *Combust. Flame* **144**, 461–475.

Warhaft, Z. 2000 Passive scalars in turbulent flows. *Annu. Rev. Fluid Mech.* **32**, 203–240.

Warnatz, J., Maas, U. & Dibble, R. W. 2006 *Combustion: Physical and Chemical Fundamentals, Modeling and Simulation, Experiments, Pollutant Formation, 4th Edition*. Springer.

Wernz, S. & Fasel, H. F. 1996 Numerical investigation of unsteady phenomena in wall jets. *AIAA paper, 96-0079* .

Wernz, S. & Fasel, H. F. 1997 Numerical investigation of forced transitional wall jets. *AIAA paper, 97-2022* .

Westbrook, C. K., Mizobuchi, Y., Poinsot, T. J., Smith, P. J. & Warnatz, J. 2005 Computational combustion. *Proc. Combust. Inst.* **30**, 125–157.

Williams, F. A. 1985 *Combustion Theory*, 2nd edn. Benjamin/Cummings.

Wygnanski, I., Katz, Y. & Horev, E. 1992 On the applicability of various scaling laws to the turbulent wall jet. *J. Fluid Mech.* **234**, 669–690.

Yu, R., Yu, J. & Bai, X.-S. 2012 An improved high-order scheme for DNS of low Mach number turbulent reacting flows based on stiff chemistry solver. *J. Comput. Phys.* **231**, 5504–5521.

Zhang, Y., Bi, W.-T., Hussain, F. & She, Z. 2014 A generalized Reynolds analogy for compressible wall-bounded turbulent flows. *J. Fluid Mech.* **739**, 392–420.

Zhou, M. D., Heine, C. & Wygnanski, I. 1996 The effects of excitation on the coherent and random motion in a plane wall jet. *J. Fluid Mech.* **310**, 1–37.